Research Article

Sobia Sultana*

Robustness and dynamical features of fractional difference spacecraft model with Mittag–Leffler stability

https://doi.org/10.1515/phys-2024-0066
received November 29, 2023; accepted July 10, 2024

Abstract: Spacecraft models that mimic the Planck satellite's behaviour have produced information on cosmic microwave background radiation, assisting physicists in their understanding of the composition and expansion of the universe. For achieving the intended formation, a framework for a discrete fractional difference spacecraft model is constructed by the use of a discrete nabla operator of variable order containing the Mittag–Leffler kernel. The efficacy of the suggested framework is evaluated employing a numerical simulation of the concerning dynamic systems of motion while taking into account multiple considerations such as exterior disruptions, parameterized variations, time-varying feedback delays, and actuator defects. The implementation of the Banach fixed-point approach provides sufficient requirements for the presence of the solution as well as a distinctive feature for such mechanisms Furthermore, the consistent stability is examined. With the aid of discrete nabla operators, we monitor the qualitative behavioural patterns of spacecraft systems to provide justification for structure's chaos. We acquire the fixed points of the proposed trajectory. At each fixed point, we calculate the eigenvalue of the spacecraft system's Jacobian matrix and check for zones of instability. The outcomes exhibit a wide range of multifaceted behaviours resulting from the interaction with various fractional orders in the offered system. To maintain stability and synchronize the system, nonlinear controllers are additionally provided. The study highlights the technique's vulnerability to fractional-order factors, resulting in exclusive, changing trends and equilibrium frameworks. Because of its diverse and convoluted behaviour, the spacecraft chaotic model is an intriguing and crucial subject for research.

Keywords: spacecraft model, fractional difference equation, chaotic attractors, actuator fault, Fault-tolerant system

*** Corresponding author: Sobia Sultana**, Department of Mathematics, Imam Mohammad Ibn Saud Islamic University, Riyadh, 11461, Saudi Arabia, e-mail: ssmahmood@imamu.edu.sa

1 Introduction

Chaotic systems are extremely responsive to initial conditions (ICs). The phenomenon is frequently referred to as the butterfly influence [1]. Chaos synchronization has garnered a lot of consideration in scientific circles since Pecora and Carroll [2] developed the notion of chaotic synchronization under various ICs. The concept behind synchronization is to take advantage of the data generated by the centralized system to regulate the slave mechanism and guarantee its results adhere to the production of the acquire mechanism asymptotically. One of the most crucial uses of chaos is the synchronization of multiple chaotic dynamical structures. Over recent decades, chaotic synchronization has emerged as an intriguing topic within the arena of scientific disciplines owing to its broad range of conceivable uses in fields including chemical processes, circuit theory, aeronautical engineering, image processing, photonics, optics, cyber security, electromagnetic flux, elasticity, and fluid systems [3]. For tackling the synchronization of alike or non-similar master-slave chaotic structures, many techniques are being developed, including active supervision techniques, adaptable control approaches, fuzzy oversight procedures, back-stepping design techniques, impulsively regulation approaches, automatic control processes, parametric feedback controlling techniques, and many more [4,5].

Whenever the settings are unidentified or change over time, adaptive synchronization is used to synchronize the same or non-identical mechanisms. Wang *et al.* [6] investigated responsive synchronization for a Chen chaotic structure *via* entirely unresolved factors. Lin *et al.* [7] contemplated the dynamic, powerful observer-based synchronization of unilaterally complemented chaotic networks with an unidentified transmit time delay. Fan *et al.* [8] presented synchronization of a family of chaotic systems

based on adaptive control design of input-to-state stability. Chen *et al.* [9] expounded the hidden extreme multistability and synchronicity of memristor-coupled non-autonomous memristive Fitzhugh–Nagumo models.

Spacecraft emergence display was recently recognized as an enabler electronic device for numerous subsequent years of missions into outer space [3,4]. This system provides multiple positive effects over an individual rocket task, involving the capacity to boost and/or facilitate outreach by means of deeper starting point assessments, a high rate of failure tolerance, real-time reconfigurability, adaptability to extremely fluctuating requirements, and lesser lifetime expenses [10]. Nevertheless, from spacecraft formation setup to transformation, interaction, and pattern generation, the entire process presents enormous obstacles [11]. For deeper patterns, spacecraft substance, dominance, energy, and interactions pose substantial barriers and orientation, transportation, and operational obligations become exceedingly complex [12–14]. Environmental perturbations resulting from the force of gravity disruption, ambient drag, ultraviolet (UV) stress, and electromagnetism may cause the spacecraft to takeoff [15]. To address these issues, novel techniques for accomplishing spacecraft creation constellations while minimizing location maintenance necessities are being requested. The manoeuvring of spacecrafts in their navigation is critical to security forces, courteousness, and research endeavours. Spacecraft framework synchronization is an active academic field [16,17]. Several methods and procedures were implemented to synchronize and regulate non-linear phenomena (spacecraft attitude), specifically responsive oversight, proactive surveillance, and control using sliding mode [18,19]. The adaptable synchronization of spacecraft behaviour and momentum-based systems are complicated topics. The spacecraft behaviour framework includes unpredictability and disruptions (both exterior and interior). It is a redundant torque structure. The disruptions in the outermost layer may encompass streamlined experiences, ultraviolet ray-compelled tensions, gravitation gradient forces, and electromagnetic instances, whereas internal fluctuations can embrace parameter unpredictability [20–22]. Spacecraft mechanism synchronization is currently employed in contemporary space-purpose theories featuring multiple spacecrafts constellations with details. This is addressed by the synchronization regulation system, which regulates the variation in oversights within spacecraft constellations. The objective is to determine the advanced version of adaptive synchronization that motivates spacecraft constellations asynchronously regarding identical briefings [23,24].

In the last century, discrete fractional (DF) calculus has grown up as an appealing study field that has sparked the fascination of researchers from multiple fields [25–32]. Their uses range from biological science to environmental science to practical scientific fields, providing useful understanding of contemporary issues [27,33]. In contrast to classical non-fractional networks, fractional platforms have proven their capacity to specify multifaceted chaotic events with more precision [34,35]. It highlights their distinctive features, such as persistent memory, transparency, and adaptability. There is currently an increase in the number of articles presented on this fascinating subject [36,37]. Pérez *et al.* [38] proposed fractional algorithms that take into account order as an indicator of space and time or additional factors. There are also processes for such fractional V–O formulations in [39–42]. Because variable-order (V–O) fractional differential equations are unable to be addressed precisely, establishing computational methods to resolve them is critical. Pérez *et al.* proposed a constant-order quantitative method combining fractional calculus and Lagrange polynomials in [38]. They generalized mathematical strategies for modelling V–O fractional differential operators regarding index, exponential, and Mittag–Leffler functions, employing the aforementioned technique [43–48].

Stability hypothesis is an extensive discipline in technology and other allied areas that studies the behaviour of dynamic structures in both linear and non-linear frameworks [49]. On the contrary, substantial advancement has been achieved concerning the stability methodology for fractional order difference equations in recent years [50]. Nonetheless, the comparable concept of a discrete-time fractional-order system continues to evolve in an intriguing manner. In addition to this, the different kinds of durability discussed for this sort of equipment are the infinite and finite stability investigated in [49,50] for discrete fractional-order difference models with non-linearities as well as time interruptions. Furthermore, You *et al.* [51] investigated Mittag–Leffler stability for fractional discrete-time systems using a fixed-point strategy. Pratap *et al.* [52] provided a class of fractional-order discrete-time complex-valued neural networks with temporal delays while addressing multiple stability specifications. In addition, Huang *et al.* [53] discuss the asynchronous stability of discrete fractional-order neural networks and offer a novel algorithm for V–O neural networks.

Numerous researchers have proposed innovative formulations of discrete-time fractional calculus that have stability properties and multiple empirical results [54,55]. In particular, Abdeljawad [56] discussed the delta and nabla Caputo fractional differences and dual identities. Abdeljawad [57] offered groundbreaking research that explored the various kernels for h-fractional differences and their fractional sums. As a consequence, this research has opened pathways for the formation of additional chaotic dynamics [57].

Abdeljawad [58] expounded the fractional difference operators with discrete generalized Mittag–Leffler kernels. Also, it investigates multiple influence methods and synchronization schemes constructed to synchronize the connections of various fractional discrete chaotic environments [59–65]. These research investigations revealed that the mechanism's behaviour is greatly reliant on the fractional order picked out, highlighting its dynamic and convoluted form, making it an exciting area for research in the discipline of fractional approaches [66–72].

In fact, most former spacecraft model studies have concentrated on classical calculus. Unfortunately, the scientific investigation of discrete fractional spacecraft models is still insufficient, with little research devoted to investigating their behaviour and attributes. Tsui and Jones [73] explored the control of higher-dimensional chaos in spacecraft attitude control problem. Kuang *et al.* [74] expounded the chaotic attitude motion of spacecrafts under small perturbation torques. Furthermore, Kuang *et al.* [75] contemplated the chaotic dynamics of an asymmetrical gyrostat. Kong *et al.* [76] described the control of chaotic attitude motion of a perturbed spacecraft, while Kumar *et al.* [77] investigated controlling and synchronization of a fractional-order chaotic spacecraft model. The research emphasizes the framework's challenging and diverse behaviour, emphasizing the importance of fractional aspects in the sophistication and adaptability of spacecraft models. A great deal of the prior study concentrated mainly on commensurate-order theories in continuous-time fractional-order models. Yet it seems that there is a substantial dearth of research regarding the influence of the incommensurate scenario on the fluidity of these models. Indeed, incommensurate order is a subset of a fractional-order structure defined by revealing the order for which the formula differs. As a result, the simulation's liberty strengthens. This points to an unresolved issue in the discipline of discrete models, especially within the setting of incommensurate fractional systems. Recognizing the functioning and features of incommensurate fractional spacecrafts may provide significant discoveries and prospective uses in a wide range of fields, including neural structures, technology, artificial intelligence, viscosity, control research, cognitive behaviour, and numerous others [20,78,79]. As a result, additional inquiry and exploration on this subject are required to identify the distinctive features and conceivable advantages of incommensurate fractional spacecraft models. It is pertinent to mention that research on discrete models with V–O has yielded inadequate findings. Huang *et al.* [53] investigated a type of variable-order recurrent neural network under the Caputo h-discrete fractional operator using fixed-point techniques and Mittag–Leffler stability specifications.

Motivated by the prior argumentation, the goal of this article is to investigate and evaluate the dynamic practices of the discrete fractional spacecraft system, which includes variable exponents. By means of an amalgamation of quantitative and qualitative inspections, we execute an extensive review of the key features of this discrete fractional spacecraft model. Moreover, we have established the existence and uniqueness of the proposed model to verify its efficacy. We investigate the chaotic behaviour of spacecraft constellations using multiple techniques, including dissipativity, fixed points, Poincaré maps, and actuator faults. The suggested system's dissipative nature (strange attractor) is defended. We acquire the proposed model's fixed points, and at every fixed point, we notice that a single of the eigenvalues of the spacecraft system's Jacobian matrix is non-negative, confirming the zone of instability. By using the oversight-control procedure, we determine the synchronization of two equivalent spacecraft constellations. These investigations provide fresh perspectives on the functioning of spacecraft networks. GPS systems, telecommunications, planet perception, and climate prediction, can all benefit from measurements. This shows the distinctiveness of our work.

The article is organized as follows: in Section 2, we outline the discrete fractional spacecraft system and provide key introductory notions concerning discrete fractional calculus. Section 3 presents a qualitative analysis of the system architecture, focusing on its facts, which is followed by an explanation of the configuration's design specifications in the second section. The dissipativeness of the system, Lyapunov exponent calculation, and phase depictions aid in this inquiry. Section 4 explores the existence and uniqueness of the discrete fractional spacecraft model. Section 5 entails applying the commensurate and incommensurate orders to determine variability and verify the existence of chaotic patterns in the system. In Section 6, we developed the robust controller model technique and synchronization has developed in view of the master and slave systems. Section 7 ends the work by indicating potential research goals.

2 Preliminaries and model description

Here, the terminology for discrete fractional calculus is offered in this part, accompanied by the subsequent notations:

$$\begin{aligned} \mathbb{N}_{\mathbf{d}} &= \{\mathbf{d}, \mathbf{d}+1, \mathbf{d}+2, \ldots\}, \\ \mathbb{N}_{\mathbf{d}}^{\mathbf{T}_1} &= \{\mathbf{d}, \mathbf{d}+1, \mathbf{d}+2, \ldots, \mathbf{T}_1\}. \end{aligned} \tag{2.1}$$

Definition 2.1. [80] For $\beta(\varpi) \in (0,1]$, $\mathbf{t} \in \mathbb{N}_{\mathbf{d}}$. Suppose there is a mapping $\Phi : \mathbb{N}_{\mathbf{d}} \mapsto \mathbb{R}$, we state the nabla fractional sum with order β

$$
\begin{aligned}
&{}_{\mathbf{d}}\nabla_{\varpi}^{-\beta}\Phi(\varpi) = \frac{1}{\Gamma(\beta(\varpi))}\sum_{\kappa=\mathbf{d}+1}^{\varpi}(\varpi-\rho(\kappa))^{\overline{\beta(\varpi)-1}}\Phi(\kappa),\\
&\rho(\kappa) = \kappa-1,\ \ \varpi \in \mathbb{N}_{\mathbf{d}+1},
\end{aligned}
\tag{2.2}
$$

where the rising mapping is defined as $\varpi^{\phi} = \frac{\Gamma(\varpi+\phi)}{\Gamma(\varpi)}$, $\phi \in \mathbb{R}$.

Definition 2.2. [80] For $\beta(\varpi) \in (0,1/2)$, $\mathbf{t} \in \mathbb{N}_{\mathbf{d}}$, $\mathbf{t} \in \mathbb{N}_{\mathbf{d}}$ and there is a mapping $\Phi : \mathbb{N}_{\mathbf{d}} \mapsto \mathbb{R}$, the left nabla Atangana–Baleanu–Caputo (ABC) fractional difference is stated as follows:

$$
\begin{aligned}
({}^{\mathrm{ABC}}_{\mathbf{d}}\nabla_{\mathbf{t}}^{\beta(\varpi)}\Phi)(\varpi) = {}&\frac{\mathbb{M}(\beta(\varpi))}{1-\beta(\varpi)}\sum_{\kappa=\mathbf{d}+1}^{\varpi}\mathcal{E}_{\overline{\beta(\varpi)}}\\
&\times\left(\frac{\beta(\varpi)}{1-\beta(\varpi)}, \varpi-\rho(\kappa)\right)\nabla\Phi(\varpi),\\
&\varpi \in \mathbb{N}_{\mathbf{d}+1},
\end{aligned}
\tag{2.3}
$$

where

$$
\mathbb{M}(\beta(\varpi)) = 1-\beta(\varpi)+\frac{\beta(\varpi)}{\Gamma(\beta(\varpi))},
\tag{2.4}
$$

and $\mathcal{E}_{\overline{\mathbf{c},\mathbf{d}}}(\Omega, \mathbf{x}_3)$ denoted the nabla discrete Mittag–Leffler mapping

$$
\begin{aligned}
&\mathcal{E}_{\overline{\mathbf{c},\mathbf{d}}}(\Omega, \mathbf{x}_3) = \sum_{\kappa\geq 0}\Omega^{\kappa}\frac{\mathbf{x}_3^{\overline{\kappa\mathbf{c}+\mathbf{d}}-1}}{\Gamma(\mathbf{c}\kappa+b_1)};\\
&|\Omega|<1;\ \mathbf{c},\mathbf{d},\mathbf{x}_3 \in \mathbb{C} \quad \text{and} \quad \Re(\mathbf{c})>0.
\end{aligned}
$$

Definition 2.3. [80] For $\beta(\varpi) \in (0,1)$ and assume that there is a left fractional sum of discrete nabla ABC-fractional V–O operator is defined as follows:

$$
\begin{aligned}
({}^{\mathrm{AB}}_{\mathbf{d}}\nabla_{\varpi}^{-\beta(\varpi)}\Phi)(\varpi) = {}&\frac{1-\beta(\varpi)}{\beta(\varpi)}\Phi(\varpi)\\
&+\frac{\beta(\varpi)}{\mathbb{M}(\beta(\varpi))}{}_{\mathbf{d}}\nabla_{\varpi}^{-\beta(\varpi)}\Phi(\varpi).
\end{aligned}
\tag{2.5}
$$

Theorem 2.1. [81] *Suppose that* $\vartheta(\zeta) = (\vartheta_1(\zeta),\ldots,\vartheta_{\mathbf{m}}(\zeta))^{\mathbf{T}}$ *and* $\Phi \in \mathbb{M}_{\mathbf{m}}(\mathbb{R})$. *The linear fractional-order discrete system's having zero steady state*:

$$
{}^{\mathrm{ABC}}_{\mathbf{d}}\nabla_{\mathbf{d}}^{\beta}\vartheta(\zeta) = \Phi\vartheta(\ell),
\tag{2.6}
$$

$\forall\zeta \in \mathbb{N}_{\mathbf{d}-1+\beta}$ *is asymptotically stable if*:

$$
\begin{aligned}
\omega_{\iota} \in \Bigg\{\omega \in \mathcal{B} : |\omega| < {}&\left(2\cos\frac{|\arg\omega|-\pi}{2-\beta}\right)^{\beta} \ \text{and}\ |\arg\omega|\\
&>\frac{\beta\pi}{2}\Bigg\},
\end{aligned}
\tag{2.7}
$$

where ω_{ι} *signified the eigenvalue.*

Lemma 2.1. *Suppose there is a* $\varpi \in \mathbb{N}_{\mathbf{d}+1}$, *then the subsequent satisfies*

$$
\sum_{\kappa=\mathbf{d}+1}^{\varpi}(\varpi-\rho(\kappa))^{\overline{\beta(\varpi)-1}} = \frac{(\varpi-\mathbf{d})^{\beta(\varpi)}}{\beta(\varpi)}.
\tag{2.8}
$$

Proof. For the first step with, we have

$$
\begin{aligned}
&\sum_{\kappa=\mathbf{d}+1}^{\varpi}(\varpi-\rho(\kappa))^{\overline{\beta(\varpi)-1}}\\
&\quad=\sum_{\kappa=\mathbf{d}+1}^{\varpi-1}(\varpi-\rho(\kappa))^{\overline{\beta(\varpi)-1}}+1^{\overline{\beta(\varpi)-1}}\\
&\quad=\sum_{\kappa=\mathbf{d}+1}^{\varpi-1}\frac{\Gamma(\varpi-\kappa+\beta(\varpi))}{\Gamma(\varpi-\kappa+1)}+\Gamma(\beta(\varpi)).
\end{aligned}
\tag{2.9}
$$

Notice that

$$
\frac{\Gamma(\kappa+1)}{\Gamma(\kappa-\iota+1)} = \frac{\kappa+2}{(\iota+1)(\kappa-\iota+1)}-\frac{\kappa+1}{(\iota+1)(\kappa-\iota)}.
\tag{2.10}
$$

Setting $\kappa = \varpi-\kappa+\beta(\varpi)-1$, $\iota = \beta(\varpi)-1$, we find

$$
\begin{aligned}
\frac{\Gamma(\varpi-\kappa+\beta(\varpi))}{\Gamma(\varpi-\kappa+1)} = {}&\frac{\Gamma(\varpi-\kappa+\beta(\varpi)+1)}{\beta(\varpi)\Gamma(\varpi-\kappa+1)}\\
&-\frac{\Gamma(\varpi-\kappa+\beta(\varpi))}{\beta(\varpi)\Gamma(\varpi-\kappa)}.
\end{aligned}
\tag{2.11}
$$

For all $\kappa \in \{\mathbf{d}+1,\ldots,\varpi-1\}$, we find

$$
\begin{aligned}
&\sum_{\kappa=\mathbf{d}+1}^{\varpi-1}\frac{\Gamma(\varpi-\kappa+\beta(\varpi))}{\Gamma(\varpi-\kappa+1)}\\
&\quad=\frac{1}{\beta(\varpi)}\Bigg\{\left(\frac{\Gamma(\varpi-\mathbf{d}+\beta(\varpi))}{\Gamma(\varpi-\mathbf{d})}-\frac{\Gamma(\varpi-\mathbf{d}+\beta(\varpi)-1)}{\Gamma(\varpi-\mathbf{d}-1)}\right)\\
&\qquad\left(\frac{\Gamma(\varpi-\mathbf{d}+\beta(\varpi)-1)}{\Gamma(\varpi-\mathbf{d}-1)}-\frac{\Gamma(\varpi-\mathbf{d}+\beta(\varpi)-2)}{\Gamma(\varpi-\mathbf{d}-2)}\right)\\
&\qquad\left(\frac{\Gamma(\varpi-\mathbf{d}+\beta(\varpi)-2)}{\Gamma(\varpi-\mathbf{d}-2)}-\frac{\Gamma(\varpi-\mathbf{d}+\beta(\varpi)-3)}{\Gamma(\varpi-\mathbf{d}-3)}\right)\\
&\qquad\vdots\\
&\qquad\left(\frac{\Gamma(\beta(\varpi)+2)}{\Gamma(2)}-\frac{\Gamma(\beta(\varpi)+1)}{\Gamma(1)}\right)\Bigg\}.
\end{aligned}
\tag{2.12}
$$

Thus, we find

$$\begin{aligned}
&\sum_{\kappa=\mathbf{d}+1}^{\varpi} (\varpi - \rho(\kappa))^{\overline{\beta(\varpi)-1}} \\
&= \frac{1}{\beta(\varpi)}\left(\frac{\Gamma(\varpi - \mathbf{d} + \beta(\varpi))}{\Gamma(\varpi - \mathbf{d})} - \Gamma(\beta(\varpi) + 1)\right) \\
&\quad + \Gamma(\beta(\varpi)) \\
&= \frac{1}{\beta(\varpi)}\left(\frac{\Gamma(\varpi - \mathbf{d} + \beta(\varpi))}{\Gamma(\varpi - \mathbf{d})}\right) \\
&= \frac{(\varpi - \mathbf{d})^{\beta(\varpi)}}{\beta(\varpi)}.
\end{aligned} \tag{2.13}$$

This completes the proof. □

Next, the rotational motion of the formula for a steadfast spacecraft [82] can be written as follows:

$$\mathcal{M} = \mathfrak{I}\theta, \tag{2.14}$$

where $\mathcal{M}$ denotes the aggregate amount of momentum performing on the the spacecraft and $\mathfrak{I}$ signifies the inertia matrix and θ is the rotational velocity.

The differentiation of the entire momentum $\mathcal{M}$ can be expressed as follows:

$$\dot{\mathcal{M}} = \mathfrak{I}\dot{\theta} + \theta \times \mathfrak{I}\theta = \hbar + \Omega, \tag{2.15}$$

where $\mathfrak{I}$ represents the balanced body's momentum tensor within the centre of mass *via* $\mathfrak{I} = \mathrm{diag}(\mathfrak{I}_{\mathbf{x}_1}, \mathfrak{I}_{\mathbf{x}_2}, \mathfrak{I}_{\mathbf{x}_3})$, the angle of rotation θ is $\theta = [\theta_1, \theta_2, \theta_3]^{\mathbf{T}}$ and the exterior disruptions torque is $\hbar = [\hbar_{\mathbf{x}_1}, \hbar_{\mathbf{x}_2}, \hbar_{\mathbf{x}_3}]^{\mathbf{T}}$ and the adjusting torque alongside $\Omega = [\Omega_1, \Omega_2, \Omega_3]^{\mathbf{T}}$.

Thus, vector product in (2.15) can be composed as the combination of the skew-symmetric cross product matrix $[\theta]$ and the vector representation $\mathfrak{I}\theta$.

$$\mathfrak{I}\dot{\theta} + \begin{pmatrix} 0 & -\theta_{\mathbf{x}_1} & \theta_{\mathbf{x}_2} \\ \theta_{\mathbf{x}_3} & 0 & -\theta_{\mathbf{x}_1} \\ -\theta_{\mathbf{x}_2} & \theta_{\mathbf{x}_2} & 0 \end{pmatrix}(\mathfrak{I}\theta) = \hbar + \Omega. \tag{2.16}$$

In view of (2.16), the rotational speed can be written in context of differential equations as follows:

$$\begin{aligned}
\mathfrak{I}_{\mathbf{x}_1}\dot{\theta}_{\mathbf{x}_1} &\equiv \theta_{\mathbf{x}_2}\theta_{\mathbf{x}_3}(\mathfrak{I}_{\mathbf{x}_2} - \mathfrak{I}_{\mathbf{x}_3}) + \hbar_{\mathbf{x}_1} + \Omega 1_{\mathbf{x}_1}, \\
\mathfrak{I}_{\mathbf{x}_2}\dot{\theta}_{\mathbf{x}_2} &\equiv \theta_{\mathbf{x}_1}\theta_{\mathbf{x}_3}(\mathfrak{I}_{\mathbf{x}_3} - \mathfrak{I}_{\mathbf{x}_1}) + \hbar_{\mathbf{x}_2} + \Omega 2_{\mathbf{x}_2}, \\
\mathfrak{I}_{\mathbf{x}_3}\dot{\theta}_{\mathbf{x}_3} &\equiv \theta_{\mathbf{x}_1}\theta_{\mathbf{x}_2}(\mathfrak{I}_{\mathbf{x}_1} - \mathfrak{I}_{\mathbf{x}_2}) + \hbar_{\mathbf{x}_3} + \Omega 3_{\mathbf{x}_3}.
\end{aligned} \tag{2.17}$$

Here, $\hbar_{\mathbf{x}_1}$, $\hbar_{\mathbf{x}_2}$ and $\hbar_{\mathbf{x}_3}$ are disrupting interference torques, while $\Omega 1_{\mathbf{x}_1}$, $\Omega 2_{\mathbf{x}_2}$, and $\Omega 3_{\mathbf{x}_3}$ constitute three influence torques. Consider that $\mathfrak{I}_{\mathbf{x}_3} < \mathfrak{I}_{\mathbf{x}_2} < \mathfrak{I}_{\mathbf{x}_1}$. Taking $\mathfrak{I}_{\mathbf{x}_1} = 3$, $\mathfrak{I}_{\mathbf{x}_2} = 2$, and $\mathfrak{I}_{\mathbf{x}_3} = 1$. The disrupting forces [3] are denoted as follows:

$$\begin{pmatrix} \hbar_{\mathbf{x}_1} \\ \hbar_{\mathbf{x}_2} \\ \hbar_{\mathbf{x}_3} \end{pmatrix} = \begin{pmatrix} -1.2 & 0 & \sqrt{6}/2 \\ 0 & 0.35 & 0 \\ -\sqrt{6} & 0 & -0.4 \end{pmatrix}\begin{pmatrix} \theta_{\mathbf{x}_1} \\ \theta_{\mathbf{x}_2} \\ \theta_{\mathbf{x}_3} \end{pmatrix}. \tag{2.18}$$

The formula for a three-dimensional in the form of chaotic spacecraft mechanism is:

$$\begin{cases}
\dot{\mathbf{x}}_1 = \varphi_{\mathbf{x}_1}\mathbf{x}_2\mathbf{x}_3 - \dfrac{1.2}{\mathfrak{I}_{\mathbf{x}_1}}\mathbf{x}_1 + \dfrac{\sqrt{6}}{2\mathfrak{I}_{\mathbf{x}_1}}\mathbf{x}_3, \\
\dot{\mathbf{x}}_2 = \varphi_{\mathbf{x}_2}\mathbf{x}_1\mathbf{x}_3 + \dfrac{0.35}{\mathfrak{I}_{\mathbf{x}_2}}\mathbf{x}_2, \\
\dot{\mathbf{x}}_3 = \varphi_{\mathbf{x}_3}\mathbf{x}_1\mathbf{x}_2 - \dfrac{\sqrt{6}}{\mathfrak{I}_{\mathbf{x}_3}}\mathbf{x}_1 - \dfrac{\sqrt{0.4}}{2\mathfrak{I}_{\mathbf{x}_3}}\mathbf{x}_3,
\end{cases} \tag{2.19}$$

where $\varphi_{\mathbf{x}_1} = \frac{\mathfrak{I}_{\mathbf{x}_2} - \mathfrak{I}_{\mathbf{x}_3}}{\mathfrak{I}_{\mathbf{x}_1}}$, $\varphi_{\mathbf{x}_2} = \frac{\mathfrak{I}_{\mathbf{x}_3} - \mathfrak{I}_{\mathbf{x}_1}}{\mathfrak{I}_{\mathbf{x}_2}}$, and $\varphi_{\mathbf{x}_3} = \frac{\mathfrak{I}_{\mathbf{x}_1} - \mathfrak{I}_{\mathbf{x}_2}}{\mathfrak{I}_{\mathbf{x}_3}}$, then we have $\sigma_{\mathbf{x}_1} = 1/3$, $\sigma_{\mathbf{x}_2} = -1$, and $\varphi_{\mathbf{x}_3} = 1$.

The spacecraft structure in all three planes has been reformulated as follows:

$$\begin{cases}
\dot{\mathbf{x}}_1 \equiv \dfrac{1}{3}\mathbf{x}_2\mathbf{x}_3 - \chi_1\mathbf{x}_1 + \dfrac{1}{\sqrt{6}}\mathbf{x}_3, \\
\dot{\mathbf{x}}_2 \equiv -\mathbf{x}_1\mathbf{x}_3 + \chi_2\mathbf{x}_2, \\
\dot{\mathbf{x}}_3 \equiv \mathbf{x}_1\mathbf{x}_2 - \sqrt{6}\,\mathbf{x}_1 - \chi_3\mathbf{x}_3,
\end{cases} \tag{2.20}$$

where the values of $\chi_1 = 0.4, \chi_2 = 0.175$, and $\chi_3 = 0.4$.

Furthermore, we present the ABC-discrete fractional form of the spacecraft model (2.20) as follows:

$$\begin{cases}
{}^{\mathrm{ABC}}_{\mathbf{d}}\nabla^{\beta(\varpi)}_{\varpi}\mathbf{x}_1(\varpi) = \dfrac{1}{3}\mathbf{x}_2(\varpi)\mathbf{x}_3(\varpi) - \chi_1\mathbf{x}_1(\varpi) \\
\qquad\qquad + \dfrac{1}{\sqrt{6}}\mathbf{x}_3(\varpi) = \mathcal{F}_1(\varpi, \mathbf{x}_1(\varpi)), \\
{}^{\mathrm{ABC}}_{\mathbf{d}}\nabla^{\beta(\varpi)}_{\varpi}\mathbf{x}_2(\varpi) = -\mathbf{x}_1(\varpi)\mathbf{x}_3(\varpi) + \chi_2\mathbf{x}_2(\varpi) \\
\qquad\qquad = \mathcal{F}_2(\varpi, \mathbf{x}_2(\varpi)), \\
{}^{\mathrm{ABC}}_{\mathbf{d}}\nabla^{\beta(\varpi)}_{\varpi}\mathbf{x}_3(\varpi) = \mathbf{x}_1(\varpi)\mathbf{x}_2(\varpi) - \sqrt{6}\,\mathbf{x}_1(\varpi) \\
\qquad\qquad - \chi_3\mathbf{x}_3(\varpi) = \mathcal{F}_3(\varpi, \mathbf{x}_3(\varpi)),
\end{cases} \tag{2.21}$$

with the aforesaid parameters and ${}^{\mathrm{ABC}}_{\mathbf{d}}\nabla^{\beta(\varpi)}_{\varpi}$ denotes the AB-discrete fractional difference of the Caputo type with V–O $\beta(\varpi) \in (0, 1)$ and $\mathbb{M}(\beta(\varpi)) = 1 - \beta(\varpi) + \frac{\beta(\varpi)}{\Gamma(\beta(\varpi))}$.

3 Qualitative analysis of fractional spacecraft model

This section investigates the requirements for dynamical evaluations of the discrete fractional spacecraft model (2.21), including dissipativity of the system, fixed points, invariancy of the $\mathbf{x}_2$-axis, and maximum Lyapunov exponents $\Omega_{\max}$.

3.1 Existence of dissipativeness

Here, the vector representation of (2.21) can be described as follows:

$$
\begin{aligned}
&{}^{ABC}_{\mathbf{d}}\nabla^{\beta(\varpi)}_{\varpi}\mathbf{Y}(\varpi+1-\beta(\varpi))\\
&\quad=\tilde{\Theta}(\varpi+1-\beta(\varpi))=\begin{pmatrix}\Theta_1(\mathbf{x}_1,\mathbf{x}_2,\mathbf{x}_3)\\ \Theta_2(\mathbf{x}_1,\mathbf{x}_2,\mathbf{x}_3)\\ \Theta_3(\mathbf{x}_1,\mathbf{x}_2,\mathbf{x}_3)\end{pmatrix},
\end{aligned}
\tag{3.1}
$$

where $\mathbf{Y}(\varpi+1-\beta(\varpi))=(\mathbf{x}_1,\mathbf{x}_2,\mathbf{x}_3)$ and

$$
\tilde{\Theta}(\mathbf{x}_1)=\begin{pmatrix}\Theta_1(\mathbf{x}_1,\mathbf{x}_2,\mathbf{x}_3)=\frac{1}{3}\mathbf{x}_2(\tau)\mathbf{x}_3(\ell)-\chi_1\mathbf{x}_1(\tau)\\ \qquad\qquad+\frac{1}{\sqrt{6}}\mathbf{x}_3(\tau)-\mathbf{x}_1(\tau)\\ \Theta_2(\mathbf{x}_1,\mathbf{x}_2,\mathbf{x}_3)=-\mathbf{x}_1(\tau)\mathbf{x}_3(\tau)+\chi_2\mathbf{x}_2(\tau)-\mathbf{x}_2(\tau)\\ \Theta_2(\mathbf{x}_1,\mathbf{x}_2,\mathbf{x}_3)=\mathbf{x}_1(\tau)\mathbf{x}_2(\tau)-\sqrt{6}\,\mathbf{x}_1(\tau)-\chi_3\mathbf{x}_3(\tau)\end{pmatrix},
\tag{3.2}
$$

where $\chi_1=0.40,\chi_2=0.175$, and $\chi_3=0.4$. We examine a particular $\Lambda(\varpi)\in\mathbb{R}^3$ domain containing a uniform boundary and $\Lambda(\varpi)=\Theta_{\varpi}(\Lambda)$, where Θ_{ϖ} is the flow velocity of $\tilde{\Theta}$.

Assume that $\mathcal{V}(\varpi)$ indicates the volume of $\Lambda(\varpi)$.

Making the use of Liouville's theorem, we have

$$
\dot{\mathcal{V}}(\varpi)=\int_{\Lambda(\varpi)}(\nabla.\ \tilde{\Theta})\mathrm{d}\mathbf{x}_1\mathrm{d}\mathbf{x}_2\mathrm{d}\mathbf{x}_3.
\tag{3.3}
$$

Thus, the divergence of the spacecraft model (2.21) is expressed as follows:

$$
\begin{aligned}
\nabla.\ \tilde{\Theta}&=\left[\frac{\partial\Theta_1}{\partial\mathbf{x}_1}+\frac{\partial\Theta_2}{\partial\mathbf{x}_2}+\frac{\partial\Theta_3}{\partial\mathbf{x}_3}\right]=-\chi_1+\chi_2-\chi_3\\
&=-0.625.
\end{aligned}
\tag{3.4}
$$

In view of (3.3) and (3.4), we attain the fractional difference equation as follows:

$$
\begin{aligned}
&{}^{ABC}_{\mathbf{d}}\nabla^{\beta(\varpi)}_{\varpi}\mathcal{V}(\varpi+1-\beta(\varpi))\\
&\quad=-0.625\mathcal{V}(\varpi+1-\beta(\varpi)).
\end{aligned}
\tag{3.5}
$$

The solution of (3.5) can be described as follows:

$$
\mathcal{V}(\varpi)=\exp(-0.625\varpi)\mathcal{V}(0).
\tag{3.6}
$$

Thus, the volumes of the beginning points decreased by exp in relation to time ϖ. $\mathcal{V}(\varpi)\mapsto 0$ when $\varpi\mapsto\infty$, ϖ increases at a pace that is exponential. This system's constraints are confined to the particular limit set that includes zero volume. The strange attractors influence the asynchronous action of a discrete fractional spacecraft model (3.6). It denotes that the framework (2.21) exhibits chaotic pattern, see Figure 1. This supports the existence of dissipative creation in discrete fractional spacecraft systems (2.21).

3.2 Equilibrium points

To investigate the dynamics of (2.21), we initially obtain the equilibrium points. First, we described the following lemma, which is mainly due to Matignon [83].

Lemma 3.1. [83] *Assume that there is a equilibrium point* $\mathbf{Y}_0$ *of the fractional-order-system and the eigenvalues of Jacobian matrix at the associated fixed points verifies the subsequent assumptions*:

$$
|\arg(eig(\mathbb{J}(\omega_\iota)))|<\beta\pi/2\ \Rightarrow\ \beta>\max\left\{\frac{2}{\pi}\arctan\left(\frac{\Im(\omega_\iota)}{\Re(\omega_\iota)}\right)\right\}.
$$

To identify the fixed points, address the subsequent expressions in (2.21) equating to zero as follows:

$$
\begin{cases}
0=\frac{1}{3}\mathbf{x}_2(\ell)\mathbf{x}_3(\ell)-\mathbf{d}\mathbf{x}_1(\ell)+\frac{1}{\sqrt{6}}\mathbf{x}_3(\ell)-\mathbf{x}_1(\ell),\\
0=-\mathbf{x}_1(\ell)\mathbf{x}_3(\ell)+b_1\mathbf{x}_2(\ell)-\mathbf{x}_2(\ell),\\
0=\mathbf{x}_1(\ell)\mathbf{x}_2(\ell)-\sqrt{6}\,\mathbf{x}_1(\ell)-\mathbf{c}\mathbf{x}_3(\ell).
\end{cases}
\tag{3.7}
$$

The expression has the fixed points:

$$
\begin{aligned}
&\tilde{\mathbf{E}}_0=(0,0,0)^{\mathbf{T}},\ \tilde{\mathbf{E}}_1=(1.1910,2.5766,0.3785)^{\mathbf{T}},\\
&\tilde{\mathbf{E}}_2=(0.1582,-1.3641,-1.5086)^{\mathbf{T}},\\
&\tilde{\mathbf{E}}_3=(-0.1582,-1.3641,1.5086)^{\mathbf{T}},\\
&\tilde{\mathbf{E}}_4=(-1.1910,2.5766,-0.3785)^{\mathbf{T}}.
\end{aligned}
$$

Therefore, the Jacobian matrix of the system (2.21) is defined as follows:

$$
\mathbb{J}(\mathbf{Y})=\begin{pmatrix}-\chi_1 & 0.33\mathbf{x}_3 & 0.33\mathbf{x}_2+1/\sqrt{6}\\ -\mathbf{x}_3 & \chi_2 & -\mathbf{x}_1\\ \mathbf{x}_2-\sqrt{6} & \mathbf{x}_1 & -\chi_3\end{pmatrix}.
\tag{3.8}
$$

The expression (3.8) at $\tilde{\mathbf{E}}_0=(0,0,0)$ can be described as follows:

$$
\mathbb{J}_{\tilde{\mathbf{E}}_0}=\begin{pmatrix}-0.4 & 0 & 0.4082\\ 0 & 0.175 & 0\\ -2.45 & 0 & -0.4\end{pmatrix}.
\tag{3.9}
$$

At $\tilde{\mathbf{E}}_0=(0,0,0)$, the eigenvalues $\omega_{01,02}=-0.40\pm 0.99\iota$ and $\omega_{03}=0.175$ demonstrate that $\tilde{\mathbf{E}}_0$ is a saddle-focus fixed point. It signifies a destabilized region.

The expression (3.8) at $\tilde{\mathbf{E}}_1=(1.1910,2.5766,0.3785)$ can be described as follows:

$$
\mathbb{J}_{\tilde{\mathbf{E}}_1}=\begin{pmatrix}-0.40 & 0.124 & 1.26\\ -0.379 & 0.175 & -1.191\\ 0.127 & 1.191 & -0.40\end{pmatrix}.
\tag{3.10}
$$

At $\tilde{\mathbf{E}}_1=(1.1910,2.5766,0.3785)$, the eigenvalues $\omega_{11}=-0.7999$, $\omega_{12}=0.0875+1.2075\iota$, and $\omega_{13}=0.0875-1.2075\iota$ demonstrate that $\tilde{\mathbf{E}}_1$ is a saddle-focus fixed point. It signifies an destabilized region.

The expression (3.8) at $\tilde{\mathbf{E}}_2=(0.1582,-1.3641,-1.5086)$ can be described as

$$
\mathbb{J}_{\tilde{\mathbf{E}}_2}=\begin{pmatrix}-0.40 & -0.498 & -0.042\\ 1.509 & 0.175 & -0.158\\ -3.814 & 0.158 & -0.40\end{pmatrix}.
\tag{3.11}
$$

At $\tilde{\mathbf{E}}_2 = (0.1582, -1.3641, -1.5086)$, the eigenvalues $\omega_{21,22} = 0.0875 \pm 0.8766\iota$, and $\omega_{23} = -0.80$ demonstrate that $\tilde{\mathbf{E}}_1$ is a saddle-focus fixed point. It signifies again an destabilized region.

Analogously, at $\tilde{\mathbf{E}}_3 = (-0.1582, -1.3641, 1.5086)$, the eigenvalues $\omega_{31,32} = 0.0875 \pm 0.8766\iota$ and $\omega_{33} = -0.80$, and $\tilde{\mathbf{E}}_4 = (-1.1910, 2.5766, -0.3785)$, the eigenvalues $\omega_{41} = -0.7999$ and $\omega_{42,43} = 0.0875 \pm 1.2075\iota$ demonstrate that $\tilde{\mathbf{E}}_3$ and $\tilde{\mathbf{E}}_4$ are saddle-focus fixed points. It identifies destabilized region. It has been illustrated in Figure 2.

3.3 The invariancy of x_2-axis

According to discrete fractional spacecraft model (2.21), it is worth mentioning that when $\mathbf{x}_1(0) = \mathbf{x}_3(0) = 0$, then $\mathbf{x}_1$ and $\mathbf{x}_3$ stay zero $\forall \varpi \in \mathbb{N}_{\mathbf{d}+1}$. Therefore, $\mathbf{x}_2$-axis signifies an orbit, which can be expressed as

$$ {}^{\mathrm{ABC}}_{\mathbf{d}}\nabla^{\beta(\varpi)}_{\varpi}\mathbf{x}_2(\varpi + 1 - \beta(\varpi)) = \chi_2\mathbf{x}_2(\varpi), $$

which yields

$$ \mathbf{x}_2(\varpi) = \exp(\chi_2\varpi)\mathbf{x}_2(0), \quad \text{for } \mathbf{x}_1 = \mathbf{x}_3 = 0. $$

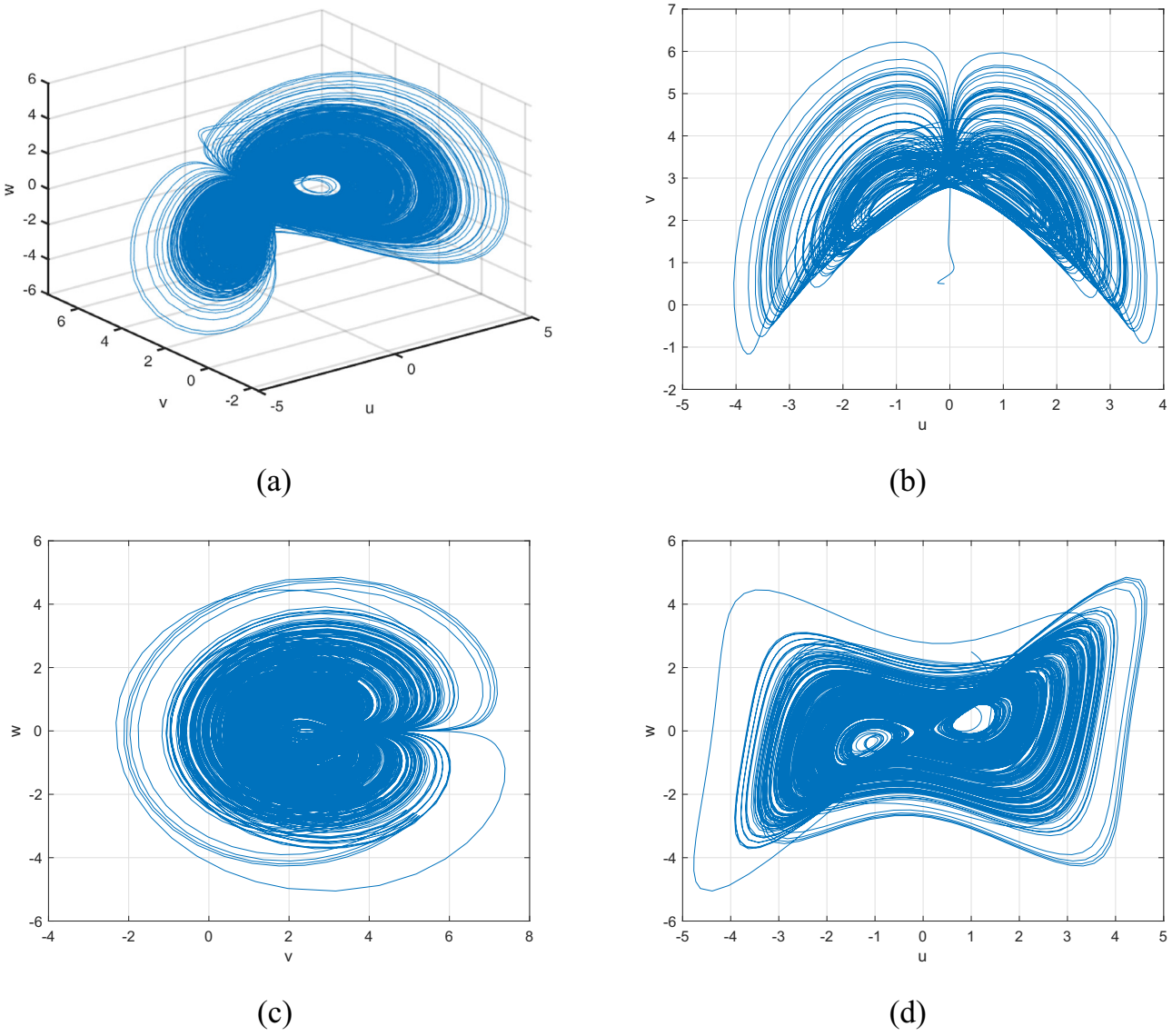

Figure 1: Phase portraits for 3D and 2D for fractional-order spacecraft model (2.21) with fractional-order $\beta = 0.96$.

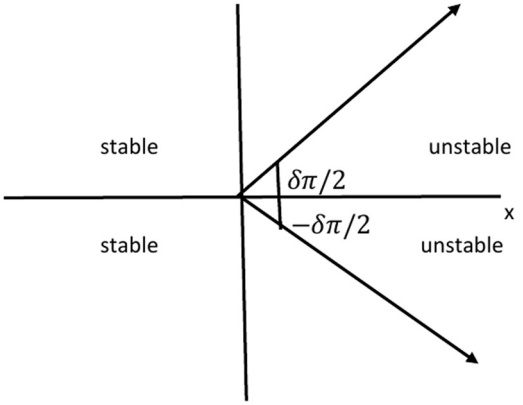

Figure 2: Stabilized zone for fractional-order system.

As a result, the $\mathbf{x}_2$-axis is an integral component of the unsteady manifold at the starting point of fixed points.

3.4 Maximum Lyapunov exponents ($\Omega_{\max}$)

Employing the system parameters for $\chi_1 = 0.40, \chi_2 = 0.175$, and $\chi_3 = 0.40$, the $\Omega_{\max}$ of discrete fractional spacecraft model (2.21) at $\sigma = 100$ can be determined using MATLAB 2023 as: $\mathbf{L}_1 = 0.13959, \mathbf{L}_2 = 0.00804$, and $\mathbf{L}_3 = -0.77267$. When we calculate the $\Omega_{\max}$ for the discrete fractional spacecraft system (2.21), we observe that one is non-negative, other is negative, and one is generally zero, indicating an essential prerequisite for system chaos. It proves that the spacecraft structures are chaotic. Figure 1 depicts it. Here, $\mathbf{L}_1 = 0.13959$ is the $\Omega_{\max}$ of spacecraft system (2.21). The total number of Lypunove exponents is calculated as $\mathbf{L}_1 + \mathbf{L}_2 + \mathbf{L}_3 = -0.604 < 0$. Finally, spacecraft model (2.21) is dissipative.

4 Existence and uniqueness

Consider the following ABC-discrete fractional variable order system is presented as follows:

$$\begin{aligned} &({}^{\mathrm{ABC}}_{\mathbf{d}}\nabla^{\beta(\varpi)}_{\varpi} y_\iota)(\varpi) = \mathcal{F}_1(\varpi, y_\iota(\varpi)),\\ &\varpi \in \mathbb{N}^{\mathbf{T}}_{\mathbf{d}} = \{\mathbf{d}, \mathbf{d}+1, \mathbf{d}+2, \ldots, \mathbf{T}\}, y_\iota(\mathbf{d}) = \mathbf{d}_0,\\ &\iota = 1, 2, 3. \end{aligned} \tag{4.1}$$

such that $\mathbf{T} \equiv \mathbf{d}(\mathrm{mod}\ 1)$, $\mathcal{F}_1(\mathbf{d}, \mathbf{x}_2(\mathbf{d})) = 0$, $\mathcal{A}\left(\frac{1-\beta(\varpi)}{\mathbb{M}(\beta(\varpi))} + \frac{(\mathbf{T}-\mathbf{d})^{\overline{\beta(\varpi)}}}{\Gamma(\beta(\varpi))\mathbb{M}(\beta(\varpi))}\right) < 1$, and $|\mathcal{F}_1(\mathbf{t}, \mathbf{x}_2) - \mathcal{F}_1(\mathbf{t}, \mathbf{y}_2)| \le \mathcal{A}|\mathbf{x}_2 - \mathbf{y}_2|$, $\mathcal{A} > 0$, where $\mathcal{F}_1 : \mathbb{N}_{\mathbf{d},b_1} \times \mathbb{R} \mapsto \mathbb{R}$ and $\mathbf{x}_2 : \mathbb{N}_{\mathbf{d},b_1} \mapsto \mathbb{R}$. Then, the system (2.21) has a unique solution of the form

$$\mathbf{x}_2(\mathbf{t}) = \mathbf{d}_0 + {}^{\mathrm{AB}}_{\mathbf{d}}\nabla_{-\beta}\mathcal{F}_1(\mathbf{t}, \mathbf{x}_2(\mathbf{t})). \tag{4.2}$$

($\mathbb{A}_1$) For every $\varpi\mathbb{N}\mathbf{d} + 1$ and suppose there is a continuous mapping $\hbar_\iota(\varpi, \mu)$, which is Lipschitz with respect to μ, $\exists \ell_\iota \in \mathbb{R}^*_+$ as follows:

$$|\hbar_\iota(\varpi, \mu) - \hbar_\iota(\varpi, \nu)| \le \ell_\iota|\mu - \nu|, \forall \mu, \nu \in \mathbb{R}, \tag{4.3}$$

where $\ell = \max_{\iota=1,\ldots,\mathbf{m}}\{\ell_\iota\}$.

($\mathbb{A}_2$) For all $\mathbf{t} \in \mathbb{N}^{\mathbf{T}}_{\mathbf{d}+1} = \{\mathbf{d}+1, \mathbf{d}+2, \ldots, \mathbf{T}\}$, there is $\mathcal{W}_\iota \in \mathbb{R}^*_+$ and $\mathcal{W}_\iota < 1$, $\iota = 1, 2, 3$ such that

$$\begin{aligned} \mathcal{W}_1 &= \left((1-\omega) + \frac{(\mathbf{T}-\mathbf{d})^{\overline{\beta}}}{\Gamma(\beta)}\right)\frac{\Gamma(\omega)\omega_1}{\Gamma(\omega)(1-\beta)+\omega},\\ \mathcal{W}_2 &= \left((1-\omega) + \frac{(\mathbf{T}-\mathbf{d})^{\overline{\beta}}}{\Gamma(\beta)}\right)\frac{\Gamma(\omega)\omega_2}{\Gamma(\omega)(1-\beta)+\omega},\\ \mathcal{W}_3 &= \left((1-\omega) + \frac{(\mathbf{T}-\mathbf{d})^{\overline{\beta}}}{\Gamma(\beta)}\right)\frac{\Gamma(\omega)\omega_3}{\Gamma(\omega)(1-\beta)+\omega}, \end{aligned} \tag{4.4}$$

where $\omega_1 = \|\mathbf{x}_1\|_\infty$, $\omega_2 = \|\mathbf{x}_2\|_\infty$, and $\omega_3 = \|\mathbf{x}_3\|_\infty$ with $\beta(\varpi) \in [\omega, \beta]$.

Theorem 4.1. *Suppose assumptions* ($\mathbb{A}_1$) *and* ($\mathbb{A}_2$) *satisfy, then ABC-discrete fractional V–O spacecraft model* (2.21) *has unique solution.*

Proof. In view of ABC-discrete fractional VO characterization, then a solution of (2.21) is

$$\begin{aligned} \mathbf{x}_1(\varpi) = \mathbf{x}_{10} &+ \frac{1-\beta(\varpi)}{\mathbb{M}(\beta(\varpi))}[\mathcal{F}_1(\varpi, \mathbf{x}_1(\varpi))]\\ &+ \frac{\beta(\varpi)}{\mathbb{M}(\beta(\varpi))}\mathbf{d}\nabla^{-\beta(\varpi)}_{\varpi}[\mathcal{F}_1(\varpi, \mathbf{x}_1(\varpi))]. \end{aligned} \tag{4.5}$$

By implemented the following norm;

$$\begin{aligned} \|\mathbf{x}_1\| &= \sup_{\varpi\in\mathbb{N}^{\mathbf{T}}_{\mathbf{d}+1}} \|\mathbf{x}_1(\varpi)\| \quad \text{and}\\ \|\mathbf{x}_1(\varpi)\| &= \max_{\ell=1,\ldots,\mathbf{m}} |\mathbf{x}_{1\ell}(\varpi)|. \end{aligned} \tag{4.6}$$

Therefore, (4.5) can be transformed into a fixed problem. Take into account the subsequent mapping:

$$\begin{aligned} \Phi(\mathbf{x}_1)(\varpi) = \mathbf{x}_1(0) &+ \frac{1-\beta(\varpi)}{\mathbb{M}(\beta(\varpi))}[\mathcal{F}_1(\varpi, \mathbf{x}_1(\varpi))]\\ &+ \frac{\beta(\varpi)}{\mathbb{M}(\beta(\varpi))\Gamma(\beta(\varpi))}\sum_{\kappa=\mathbf{d}+1}^{\varpi}\\ &\times (\varpi - \rho(\kappa))^{\overline{\beta(\varpi-1)}}[\mathcal{F}_1(\kappa, \mathbf{x}_1(\kappa))], \end{aligned} \tag{4.7}$$

where $\Phi\mathbf{x}_1 = (\Phi_1\mathbf{x}_1, \Phi_2\mathbf{x}_{12}, \ldots, \Phi_{\mathbf{m}}\mathbf{x}_{1\mathbf{m}})$ and $\Phi_\ell\mathbf{x}_{1\ell}$ is stated as:

$$\begin{aligned} \Phi_\ell\mathbf{x}_{1\ell}(\varpi) = \mathbf{x}_{1\ell 0} &+ \frac{1-\beta(\varpi)}{\mathbb{M}(\beta(\varpi))}\sum_{\jmath=1}^{\mathbf{m}}\mathcal{F}_{1\jmath}(\varpi, \mathbf{x}_{1\jmath}(\varpi))\\ &+ \frac{\beta(\varpi)}{\mathbb{M}(\beta(\varpi))\Gamma(\beta(\varpi))}\sum_{\kappa=\mathbf{d}+1}^{\varpi}\\ &\times (\varpi - \rho(\kappa))^{\overline{\beta(\varpi-1)}}\sum_{\jmath=1}^{\mathbf{m}}\mathcal{F}_{1\jmath}(\kappa, \mathbf{x}_{1\jmath}(\kappa)). \end{aligned} \tag{4.8}$$

For every pair of distinct mappings $\mathbf{x}_1, \varpi \in \mathbb{R}^{\mathbf{m}}$, we have

$$\begin{aligned}
&|\Phi_\ell \mathbf{x}_{1\ell}(\varpi) - \Phi_\ell \mu_\ell(\varpi)| \\
&= \Bigg| \frac{1-\beta(\varpi)}{\mathbb{M}(\beta(\varpi))} \sum_{\jmath=1}^{\mathbf{m}} (\mathcal{F}_{1\jmath}(\varpi, \mathbf{x}_{1\jmath}(\varpi)) \\
&\quad - \mathcal{F}_{1\jmath}(\varpi, \mu_\jmath(\varpi))) \\
&\quad + \frac{\beta(\varpi)}{\mathbb{M}(\beta(\varpi))\Gamma(\beta(\varpi))} \sum_{\kappa=\mathbf{d}+1}^{\varpi} (\varpi - \rho(\kappa))^{\overline{\beta(\varpi-1)}} \\
&\quad \times \sum_{\jmath=1}^{\mathbf{m}} (\mathcal{F}_{1\jmath}(\kappa, \mathbf{x}_{1\jmath}(\kappa)) - \mathcal{F}_{1\jmath}(\kappa, \mu_\jmath(\kappa))) \Bigg| \\
&\le \frac{1-\beta(\varpi)}{\mathbb{M}(\beta(\varpi))} \sum_{\jmath=1}^{\mathbf{m}} |(\mathcal{F}_{1\jmath}(\varpi, \mathbf{x}_{1\jmath}(\varpi)) \\
&\quad - \mathcal{F}_{1\jmath}(\varpi, \mu_\jmath(\varpi)))| \\
&\quad + \frac{\beta(\varpi)}{\mathbb{M}(\beta(\varpi))\Gamma(\beta(\varpi))} \sum_{\kappa=\mathbf{d}+1}^{\varpi} (\varpi - \rho(\kappa))^{\overline{\beta(\varpi-1)}} \\
&\quad \times \sum_{\jmath=1}^{\mathbf{m}} |(\mathcal{F}_{1\jmath}(\kappa, \mathbf{x}_{1\jmath}(\kappa)) - \mathcal{F}_{1\jmath}(\kappa, \mu_\jmath(\kappa)))|,
\end{aligned} \tag{4.9}$$

which leads us to

$$\begin{aligned}
&\max_{\ell=1,\dots,\mathbf{m}} |\Phi_\ell \mathbf{x}_{1\ell}(\varpi) - \Phi_\ell \mu_\ell(\varpi)| \\
&\le \frac{1-\beta(\varpi)}{\mathbb{M}(\beta(\varpi))} [\omega_1 \max_{\ell=1,\dots,\mathbf{m}} |\mathbf{x}_{1\ell}(\varpi) - \mu_\ell(\varpi)|] \\
&\quad + \frac{\beta(\varpi)}{\mathbb{M}(\beta(\varpi))\Gamma(\beta(\varpi))} \sum_{\kappa=\mathbf{d}+1}^{\varpi} (\varpi - \rho(\kappa))^{\overline{\beta(\varpi-1)}} \\
&\quad \times [\omega_1 \max_{\ell=1,\dots,\mathbf{m}} |\mathbf{x}_{1\ell}(\kappa) - \mu_\ell(\kappa)|].
\end{aligned} \tag{4.10}$$

Making the use of Lemma 2.1, we have

$$\begin{aligned}
&\|\Phi \mathbf{x}_1 - \Phi\varpi\| \\
&= \sup_{\varpi \in \mathbb{N}_{\mathbf{d}+1}^{\mathbf{T}}} [\max_{\ell=1,\dots,\mathbf{m}} |\Phi_\ell \mathbf{x}_{1\ell}(\varpi) - \Phi_\ell \mu_\ell(\varpi)|] \\
&\le \Bigg[\frac{(1-\omega)\Gamma(\omega)}{\Gamma(\omega)(1-\beta)+\omega} \\
&\quad + \frac{\beta\Gamma(\omega)}{\Gamma(\beta)(\Gamma(\omega+1)(1-\beta)+\omega)} \sup_{\varpi \in \mathbb{N}_{\mathbf{d}+1}^{\mathbf{T}}} \\
&\quad \times \sum_{\kappa=\mathbf{d}+1}^{\varpi} (\varpi - \rho(\kappa))^{\overline{\beta(\varpi-1)}} \Bigg] \omega_1 \|\mathbf{x}_1 - \varpi\| \\
&\le (1-\omega) + \frac{1}{\Gamma(\beta)} \sup_{\varpi \in \mathbb{N}_{\mathbf{d}+1}^{\mathbf{T}}} (\varpi - \mathbf{d})^{\overline{\beta(\varpi)}} \\
&\quad \times \frac{\Gamma(\omega)\omega_1}{\Gamma(\omega)(1-\beta)+\omega} \|\mathbf{x}_1 - \varpi\| \\
&\le \left[(1-\omega) + \frac{(\mathbf{T}-\mathbf{d})^{\overline{\beta}}}{\Gamma(\beta)} \right] \frac{\Gamma(\omega)\omega_1}{\Gamma(\omega)(1-\beta)+\omega} \|\mathbf{x}_1 - \varpi\| \\
&= \mathcal{W}_1 \|\mathbf{x}_1 - \varpi\|.
\end{aligned} \tag{4.11}$$

Analogously, we have

$$\begin{aligned}
\|\Phi \mathbf{x}_2 - \Phi\varpi\| &\le \left[(1-\omega) + \frac{(\mathbf{T}-\mathbf{d})^{\overline{\beta}}}{\Gamma(\beta)} \right] \\
&\quad \times \frac{\Gamma(\omega)\omega_2}{\Gamma(\omega)(1-\beta)+\omega} \|\mathbf{x}_2 - \varpi\| \\
&= \mathcal{W}_2 \|\mathbf{x}_2 - \varpi\|, \\
\|\Phi \mathbf{x}_3 - \Phi\varpi\| &\le \left[(1-\omega) + \frac{(\mathbf{T}-\mathbf{d})^{\overline{\beta}}}{\Gamma(\beta)} \right] \\
&\quad \times \frac{\Gamma(\omega)\omega_3}{\Gamma(\omega)(1-\beta)+\omega} \|\mathbf{x}_3 - \varpi\| \\
&= \mathcal{W}_3 \|\mathbf{x}_3 - \varpi\|.
\end{aligned} \tag{4.12}$$

In view of supposition $(\mathbb{A}_2)$ that $\mathcal{W}_\iota$, $\iota = 1, 2, 3$; thus, the mapping Φ is a contraction on $\mathbb{C}(\mathbb{N}_{\mathbf{d}+1}^{\mathbf{T}}, \mathbb{R}^{\mathbf{m}})$. This demonstrates that discrete fractional spacecraft model (2.21) has a unique fixed point in accordance to the Banach fixed-point principle, indicating the uniqueness of the solution, which concludes our result. □

Our next result is the stability analysis of the discrete fractional spacecraft model (2.21).

Definition 4.1. [84] For initial time of the discrete variable order spacecraft model (2.21) having nabla discrete Mittag–Leffler kernel is adjusted as $\mathbf{d}$. For any $\varepsilon > 0$, there are two fixed terms β_ε and $\mathbf{T}$, then (2.21) is said to be uniformly stable if $\beta_\varepsilon \in (0, \varepsilon)$, $\mathbf{T} > 0$ and $\varpi \in \mathbb{N}_{\mathbf{d}+1}^{\mathbf{T}} = \{\mathbf{d}+1, \mathbf{d}+2, \dots, \mathbf{T}\}$ and for every two solutions $\zeta(\varpi, \mathbf{d}, \Phi)$ and $\varpi(\varpi, \mathbf{d}, \psi)$ supplemented ICs $\zeta_0 = \Phi$ and $\varpi_0 = \psi$ such that $\|\Phi - \psi\| < \beta_\varepsilon \Rightarrow \|\zeta - \mu\| < \varepsilon$.

Theorem 4.2. *Assume that the supposition* $(\mathbb{A}_1)$ *and* $(\mathbb{A}_2)$ *are satisfied, if*

$$\frac{1}{1-\mathcal{W}_\iota} < \frac{\varepsilon}{\beta}, \iota = 1, 2, 3, \tag{4.13}$$

then (2.21) *is uniformly stable.*

Proof. Assume that $\zeta(\varpi), \mu(\varpi) \in \mathbb{R}^{\mathbf{m}}$ be two distinct solutions of (2.21) supplemented with ICs ζ_0 and μ_0.Taking $\Phi = \zeta_0$ and $\Phi = \mu_0$, then spacecraft system (2.21) can be expressed as follows:

$$\begin{aligned}
&{}^{\mathrm{ABC}}_{\mathbf{d}}\nabla_{\varpi}^{\beta(\varpi)}(\zeta(\varpi) - \mu(\varpi)) \\
&\quad = \Phi - \psi - \chi(\mathcal{F}_1(\varpi, \zeta(\varpi)) - \mathcal{F}_1(\varpi, \mu(\varpi))),
\end{aligned} \tag{4.14}$$

equivalently,

$$\begin{aligned}
(\zeta(\varpi) - \mu(\varpi)) &= \Phi - \psi + \frac{1-\beta(\varpi)}{\mathbb{M}(\beta(\varpi))} \\
&\quad \times [-\chi_1(\mathcal{F}_1(\varpi, \zeta(\varpi)) - \mathcal{F}_1(\varpi, \mu(\varpi)))] \\
&\quad + \frac{\beta(\varpi)}{\mathbb{M}(\beta(\varpi)\Gamma(\beta(\varpi)))} \\
&\quad \times \sum_{\kappa=\mathbf{d}+1}^{\varpi} (\varpi - \rho(\kappa))^{\overline{\beta(\varpi)-1}} \\
&\quad \times [-\chi_1(\mathcal{F}_1(\kappa, \zeta(\kappa)) - \mathcal{F}_1(\kappa, \varpi(\kappa)))].
\end{aligned} \tag{4.15}$$

Considering assumption ($\mathbb{A}_1$), we find that

$$\begin{aligned}
&|\zeta_\ell(\varpi) - \mu_\ell(\varpi)| \\
&= \Bigg| \Phi_\ell - \psi_\ell + \frac{1-\beta(\varpi)}{\mathbb{M}(\beta(\varpi))} \\
&\quad \times \left[-\chi_1 \sum_{\jmath=1}^{\mathbf{m}} (\mathcal{F}_{1\jmath}(\varpi, \zeta_\jmath(\varpi)) - \mathcal{F}_{1\jmath}(\varpi, \mu_\jmath(\varpi))) \right] \\
&\quad - \chi_1 \frac{\beta(\varpi)}{\mathbb{M}(\beta(\varpi))\Gamma(\beta(\varpi))} \\
&\quad \times \sum_{\kappa=\mathbf{d}+1}^{\varpi} (\varpi - \rho(\kappa))^{(\beta(\varpi)-1)} \\
&\quad \times \sum_{\jmath=1}^{\mathbf{m}} (\mathcal{F}_{1\jmath}(\kappa, \zeta_\jmath(\kappa)) - \mathcal{F}_{1\jmath}(\kappa, \mu_\jmath(\kappa))) \Bigg| \\
&\le |\Phi_\ell - \psi_\ell| + \frac{1-\beta(\varpi)}{\mathbb{M}(\beta(\varpi))} \\
&\quad \times \left[\chi_1 \sum_{\jmath=1}^{\mathbf{m}} |\mathcal{F}_{1\jmath}(\varpi, \zeta_\jmath(\varpi)) - \mathcal{F}_{1\jmath}(\varpi, \mu_\jmath(\varpi))| \right] \\
&\quad + \chi_1 \frac{\beta(\varpi)}{\mathbb{M}(\beta(\varpi))\Gamma(\beta(\varpi))} \sum_{\kappa=\mathbf{d}+1}^{\varpi} (\varpi - \rho(\kappa))^{\overline{\beta(\varpi)-1}} \\
&\quad \times \sum_{\jmath=1}^{\mathbf{m}} |\mathcal{F}_{1\jmath}(\kappa, \zeta_\jmath(\kappa)) - \mathcal{F}_{1\jmath}(\kappa, \mu_\jmath(\kappa))|.
\end{aligned} \tag{4.16}$$

Furthermore, applying assumption ($\mathbb{A}_2$), we have

$$\begin{aligned}
\|\zeta - \mu\| &\le \|\Phi - \psi\| + \sup_{\varpi \in \mathbb{N}_{\mathbf{d}+1}} \frac{1-\beta(\varpi)}{\mathbb{M}(\beta(\varpi))} \chi_1 \|\zeta - \mu\| \\
&\quad + \sup_{\varpi \in \mathbb{N}_{\mathbf{d}+1}} \left[\frac{\beta(\varpi)}{\mathbb{M}(\beta(\varpi))\Gamma(\beta(\varpi))} \sum_{\kappa=\mathbf{d}+1}^{\varpi} \right. \\
&\quad \left. \times (\varpi - \rho(\kappa))^{\overline{\beta(\varpi)-1}} \right] \chi_1 \|\zeta - \mu\| \\
&\le \|\Phi - \varpi\| + \frac{(1-\omega)\Gamma(\omega)}{\Gamma(\omega)(1-\beta+\omega)} \chi_1 \|\zeta - \mu\| \\
&\quad + \frac{\Gamma(\omega)}{\Gamma(\beta)\Gamma(\omega+1)(1-\beta)+\omega} \sum_{\kappa=\mathbf{d}+1}^{\varpi} \sup_{\varpi \in \mathbb{N}_{\mathbf{d}+1}} \\
&\quad \times (\varpi - \mathbf{d})^{\overline{\beta(\varpi)}} \chi_1 \|\zeta - \varpi\| \\
&= \|\zeta - \mu\| + \frac{\Gamma(\omega)\chi_1}{\Gamma(\omega)(1-\beta)+\omega} \\
&\quad \times \left[1 - \omega + \frac{(\mathbf{T} - \mathbf{d})^{\bar{\beta}}}{\Gamma(\beta)} \right] \|\zeta - \mu\| \\
&\le \frac{1}{1 - \frac{\Gamma(\omega)\chi_1}{\Gamma(\omega)(1-\beta)+\omega} \left[1 - \omega + \frac{(\mathbf{T}-\mathbf{d})^{\bar{\beta}}}{\Gamma(\beta)} \right]} \|\Phi - \psi\|.
\end{aligned} \tag{4.17}$$

Consequently, we have

$$\|\zeta - \mu\| \le \frac{1}{1 - \mathcal{W}_1} \|\Phi - \psi\|. \tag{4.18}$$

Analogously, we can find

$$\begin{aligned}
\|\zeta - \mu\| &\le \frac{1}{1 - \mathcal{W}_2} \|\Phi - \psi\|, \\
\|\zeta - \mu\| &\le \frac{1}{1 - \mathcal{W}_3} \|\Phi - \psi\|.
\end{aligned} \tag{4.19}$$

Thus, we determine that for any $\varepsilon > 0$, $\exists\, \beta_\varepsilon = (1 - \mathcal{W}_\iota)\varepsilon$, $\iota = 1, 2, 3$, where if $\|\Phi - \psi\| < \beta$, then $\|\zeta - \mu\| < \varepsilon$ and according to Definition 4.1, (2.21) is uniformly stable, and thus, the proof is complete. □

5 Numerical experimentation for the proposed model

In the following part, the focus is on the novel investigation of how the discrete fractional spacecraft model (2.21) behaves. The evaluation will include both commensurate and incommensurate orders. We will use a variety of computational resources for displaying phase portraits and poincaré maps.

5.1 Commensurate V–O

In this section, we will elaborate on the various properties of the commensurate order for the discrete fractional spacecraft system (2.21). It is essential to comprehend that a commensurate-order fractional system consists of formulas with similar orders. To achieve this, we shall subsequently provide the numerical calculation, which originates from Theorem 4.1 and will be provided as follows:

$$\begin{cases}
\mathbf{x}_1(\ell) = \mathbf{x}_1(0) + \frac{1-\beta(\ell)}{\mathbb{M}(\beta(\ell))} \\
\left[\frac{1}{3}\mathbf{x}_2(\ell)\mathbf{x}_3(\ell) - \chi_1 \mathbf{x}_1(\ell) + \frac{1}{\sqrt{6}}\mathbf{x}_3(\ell) \right] \\
+ \frac{\beta(\ell)}{\mathbb{M}(\beta(\ell))} \sum_{\kappa=1}^{\ell} \frac{\Gamma(\ell - \kappa + \beta(\ell))}{\Gamma(\ell - \kappa + 1)} \\
\left[\frac{1}{3}\mathbf{x}_2(\kappa)\mathbf{x}_3(\kappa) - \chi_1 \mathbf{x}_1(\kappa) + \frac{1}{\sqrt{6}}\mathbf{x}_3(\kappa) \right], \\
\mathbf{x}_2(\ell) = \mathbf{x}_2(0) + \frac{1-\beta(\ell)}{\mathbb{M}(\beta(\ell))} \\
[-\mathbf{x}_1(\ell)\mathbf{x}_3(\ell) + \chi_2 \mathbf{x}_2(\ell)] \\
+ \frac{\beta(\ell)}{\mathbb{M}(\beta(\ell))} \sum_{\kappa=1}^{\ell} \frac{\Gamma(\ell - \kappa + \beta(\ell))}{\Gamma(\ell - \kappa + 1)} \\
[-\mathbf{x}_1(\kappa)\mathbf{x}_3(\kappa) + \chi_2 \mathbf{x}_2(\kappa)], \\
\mathbf{x}_3(\ell) = \mathbf{x}_3(0) + \frac{1-\beta(\ell)}{\mathbb{M}(\beta(\ell))} \\
[\mathbf{x}_1(\ell)\mathbf{x}_2(\ell) - \sqrt{6}\,\mathbf{x}_1(\ell) - \chi_3 \mathbf{x}_3(\ell)] \\
+ \frac{\beta(\ell)}{\mathbb{M}(\beta(\ell))} \sum_{\kappa=1}^{\ell} \frac{\Gamma(\ell - \kappa + \beta(\ell))}{\Gamma(\ell - \kappa + 1)} \\
[\mathbf{x}_1(\kappa)\mathbf{x}_2(\kappa) - \sqrt{6}\,\mathbf{x}_1(\kappa) - \chi_3 \mathbf{x}_3(\kappa)], \\
\mathbb{M}(\beta(\ell)) = 1 - \beta(\ell) + \frac{\beta(\ell)}{\Gamma(\beta(\ell))}, \ell \ge 1.
\end{cases} \tag{5.1}$$

Choosing $\mathbf{x}_1(0) = 2.5$, $\mathbf{x}_2(0) = 1.5$, $\mathbf{x}_3(0) = -1.5$, and the values of $\chi_1 = 0.4$, $\chi_2 = 0.175$, and $\chi_3 = 0.4$, we visualize

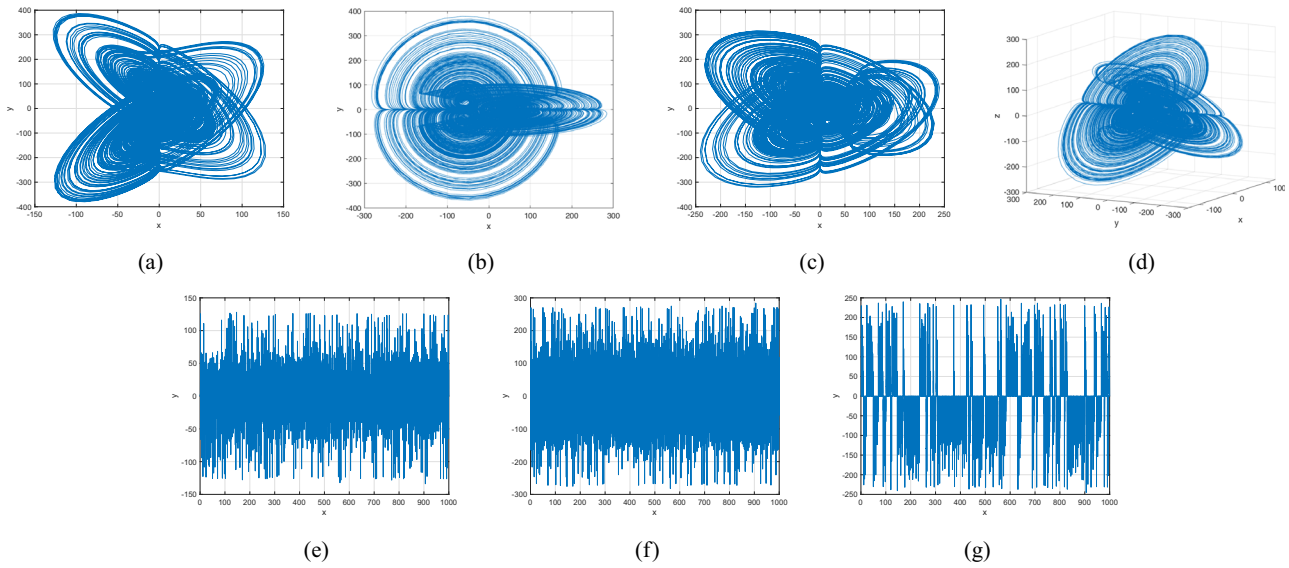

Figure 3: Phase portraits for 2D and 3D discrete fractional spacecraft model (5.1) with V–O $\beta(\varpi) = 1$.

various chaotic attractors of (5.1), which connect to the commensurate-orders $\beta(\varpi) = 1$, $\beta(\varpi) = 0.96$, $\beta(\varpi) = 0.97 + 0.03 \times \tanh(\mathbf{t}/10)$, $\beta(\varpi) = 0.97 + 0.03 \times \sin(\varpi/10)$, and $\beta(\varpi) = \frac{1}{10}(9 + \cos(\varpi/10))$ as illustrated in Figures 3–7. The parameter's structures and the commensurate-order β clearly influence the configurations of the commensurate-order discrete fractional spacecraft model (5.1). In fact, as the commensurate-order β and parameters of the system decline, the commensurate-order discrete fractional spacecraft model (5.1) exhibits an increasingly large chaotic domain. As a result, increasingly complicated resonances develop, and the mechanism's behaviour grows more unpredictable. The interaction between DFO and framework variables has an enormous effect on dynamic behaviour, and such modifications may result in a broader spectrum of chaotic structure and convoluted pathways that comprise the discrete fractional spacecraft model (5.1).

Presently, alongside $\beta(\varpi)$Âă as the significant parameter, the chaotic illustration can be utilized to show the changes in the behaviours of the commensurate discrete fractional spacecraft model (5.1) as the order $\beta(\varpi)$ fluctuates from $\beta(\varpi) = 1 - \cos^2 \varpi/2$ to $\tanh(\varpi + 1)$. The hyper-

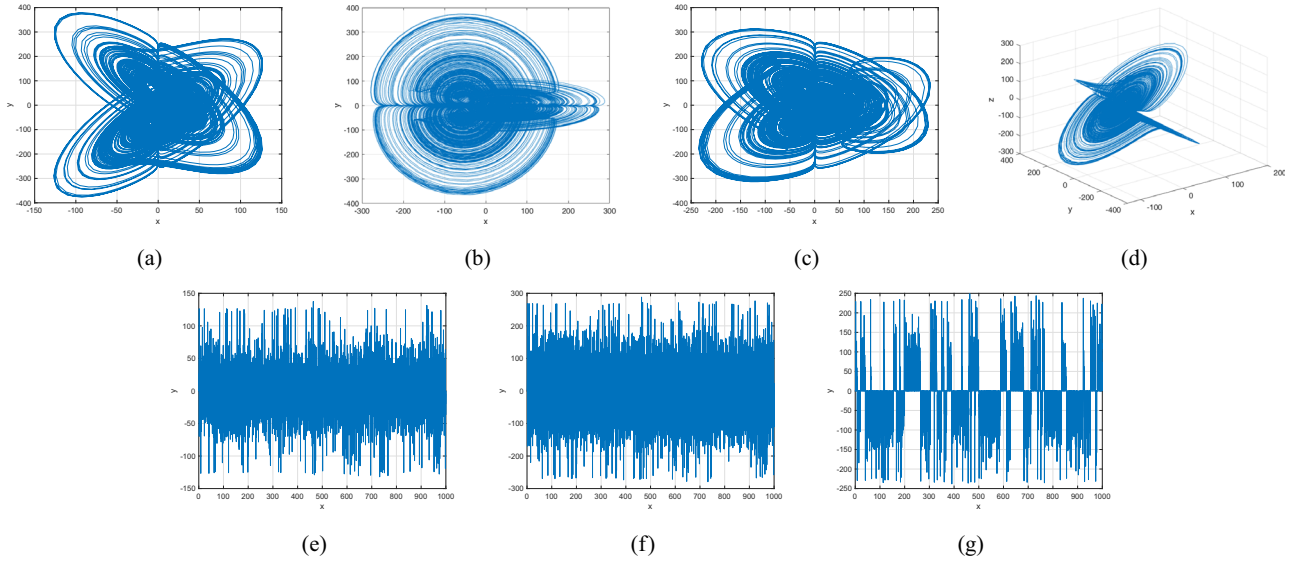

Figure 4: Phase portraits for 2D and 3D discrete fractional spacecraft model (5.1) with V–O $\beta(\varpi) = 0.96$.

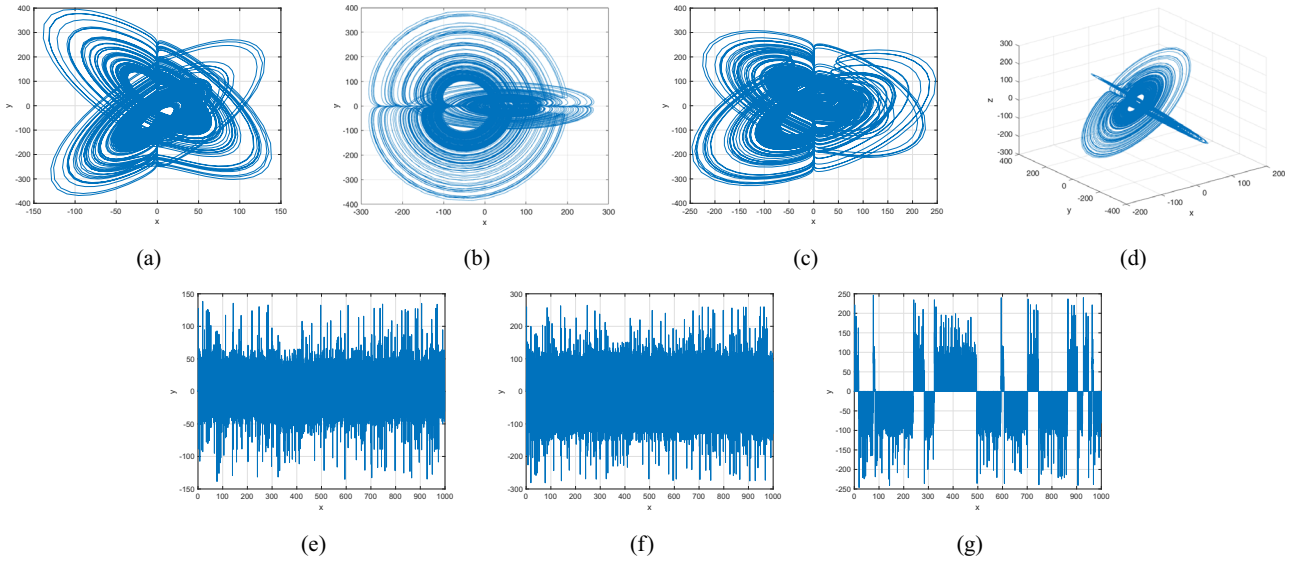

Figure 5: Phase portraits for 2D and 3D discrete fractional spacecraft model (5.1) with V–O $\beta(\varpi) = 0.97 + 0.03\tanh(\varpi/10)$.

chaos are depicted in Figures 8 and 9, respectively. We are able to observe that modifying the commensurate order investigates an extensive variety of unpredictable features (chaotic and periodic) of the fractional model in relation to the commensurate-order $\beta(\varpi)$. In particular, there are two types of domains in which the structure fluctuates chaotically and domains in which the framework rotates frequently. When $\beta(\varpi) = 1 - \cos^2 \varpi/2$ recurring views alongside various period orbits show up accompanied by an insignificant chaotic movement in the time range $(0.03, 0.20)$. We can see variations within chaotic and consistent pathways in the configurations of the commensurate-order discrete fractional spacecraft when $\beta(\varpi) = \frac{100 + 99\exp(-\varpi/4)}{100(1+\exp(-\varpi/4))}$. The chaos varies within negative and non-negative readings throughout the process, demonstrating adjustments within chaos and non-chaotic behaviours in the framework (Figure 10). The pathways of the commensurate-order discrete fractional spacecraft model (5.1) indicate chaotic behaviour when the commensurate-order is $\beta(\varpi) = \frac{1}{100}(97 + 3\cos(\varpi/10))$, and various periods show an orbital revolution, demonstrating the framework's equilibrium (Figure 11). Following that, for the aforementioned V–O $\beta(\varpi)$, chaotic gestures comeback, with an upsurge in the curve (Figures 7 and 8), demonstrating irregularities throughout the

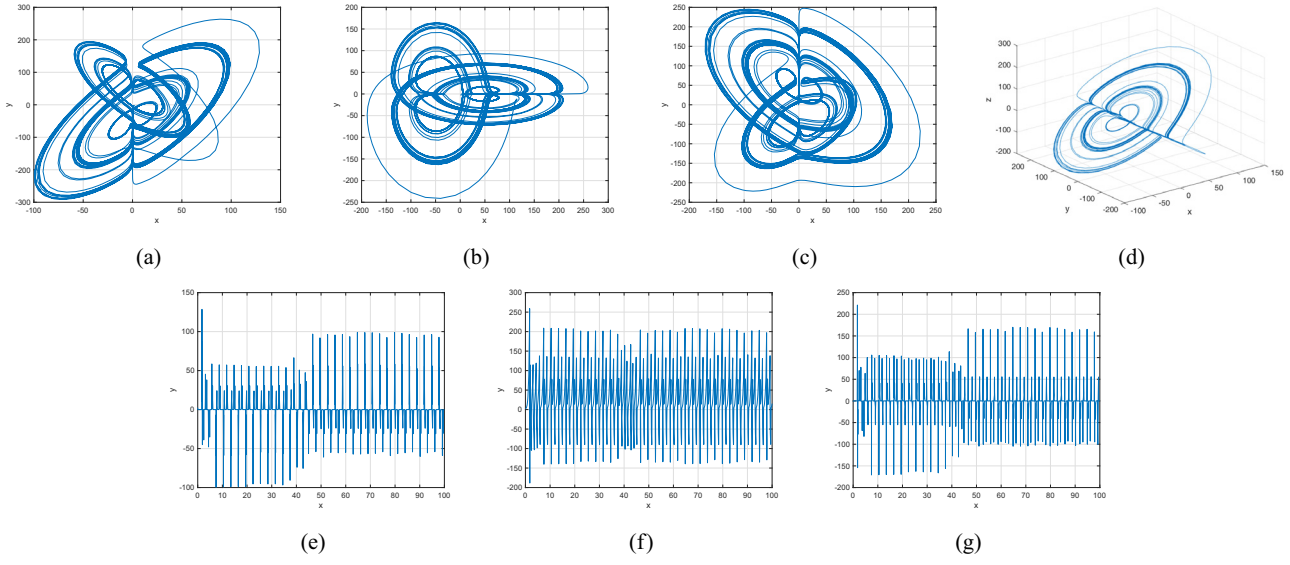

Figure 6: Phase portraits for 2D and 3D discrete fractional spacecraft model (5.1) with V–O $\beta(\varpi) = 0.97 + 0.03\sin(\varpi/10)$.

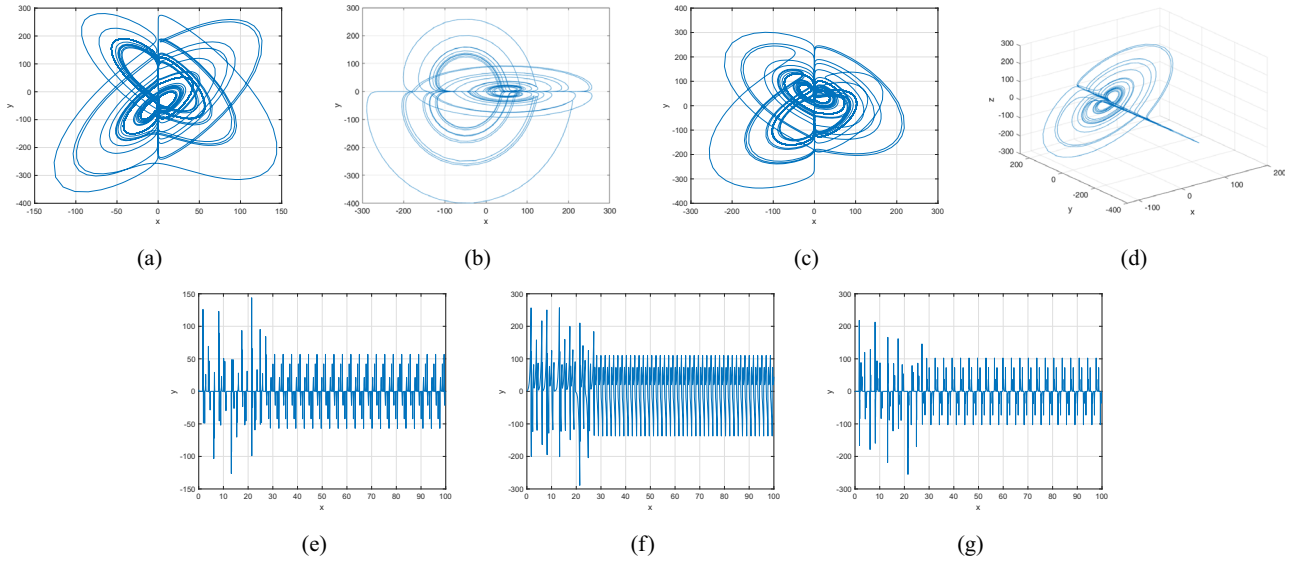

Figure 7: Phase portraits for 2D and 3D discrete fractional spacecraft model (5.1) with fractional-order $\beta(\varpi) = \frac{1}{10}(9 + \cos(\varpi/10))$.

pathways of the commensurate-order discrete fractional spacecraft model (5.1). This confirms the outlined behavioural characteristics, delivering supplementary proof for the framework's multifaceted and intricate behaviour and affirming the system's responsiveness to adjustments in the commensurate-order value β. Moreover, it is possible to determine that in situations where the $\beta(\varpi)$ is declining from 1, the corresponding discrete fractional spacecraft model (5.1) displays periodic fluctuations. Whenever the order is non-negative, the existence of chaotic fluctuations is deduced. Figures 3–11(e)–(g) depict the isolated time progression of the configurations $\mathbf{x}_1$, $\mathbf{x}_2$, and $\mathbf{x}_3$ in the proposed commensurate map to provide an extensive overview of these features. The pathways noticed within the identified commensurate system transform into chaotic fluctuations and recurring behaviours as the commensurate-order $\beta(\varpi)$ fluctuates, as shown in the diagrams. The findings highlight the mechanism's responsiveness to alterations in $\beta(\varpi)$ and indicate the extensive and intricate nature of the constantly changing features in the discrete fractional spacecraft commensurate-order model (5.1).

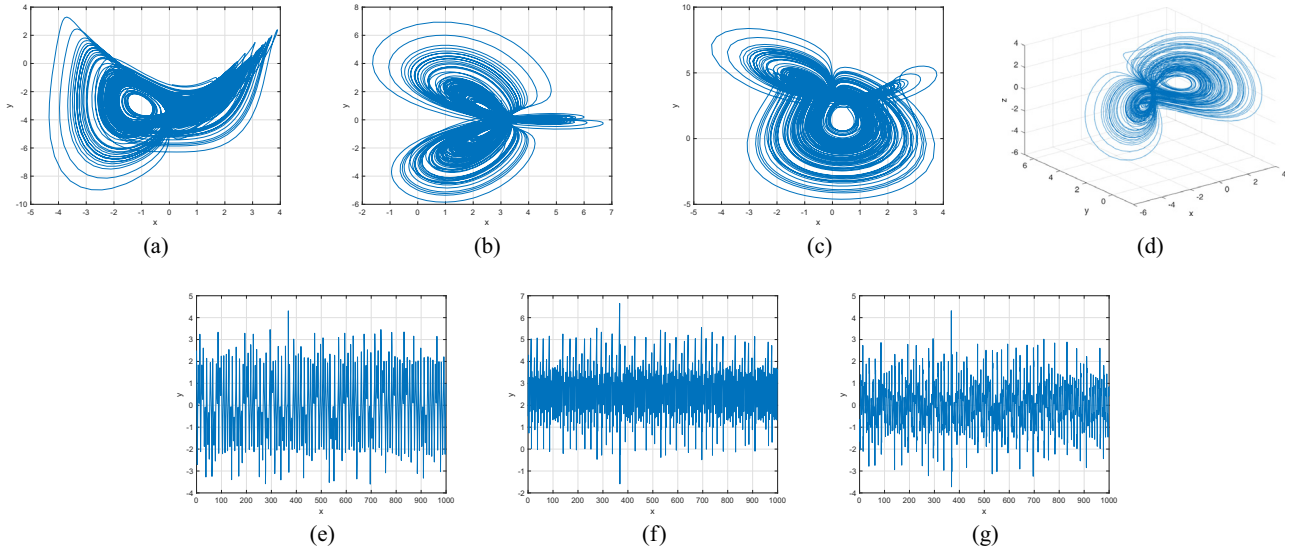

Figure 8: Phase portraits for 2D and 3D discrete fractional spacecraft model (5.1) with fractional-order $\beta(\varpi) = 1 - \cos^2 \varpi/2$.

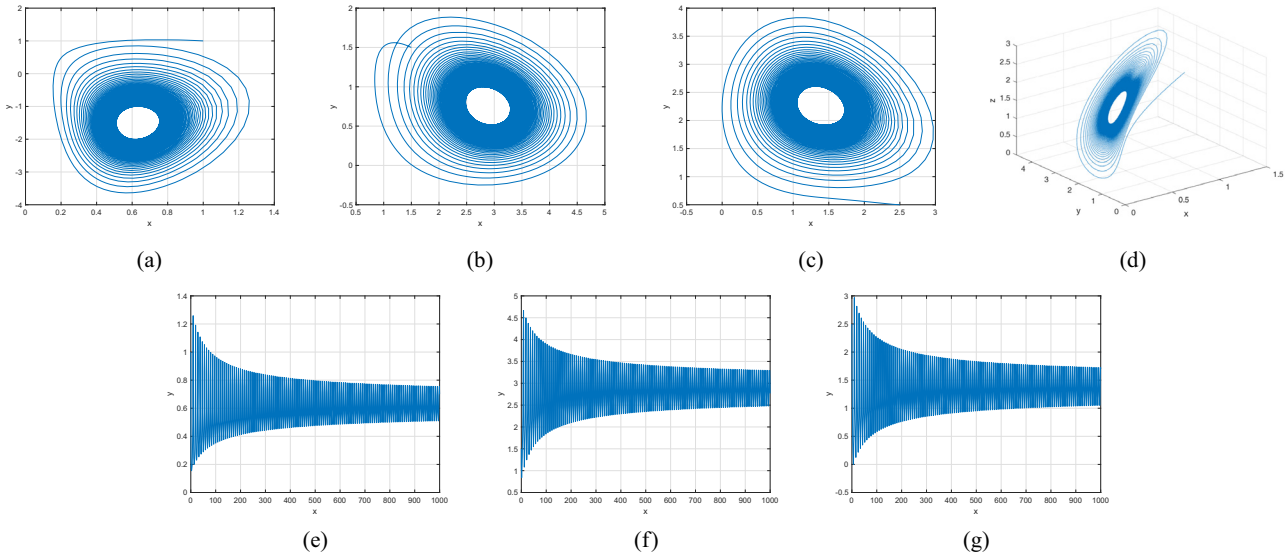

Figure 9: Phase portraits for 2D and 3D discrete fractional spacecraft model (5.1) with fractional-order $\beta(\varpi) = \tanh(\varpi + 1)$.

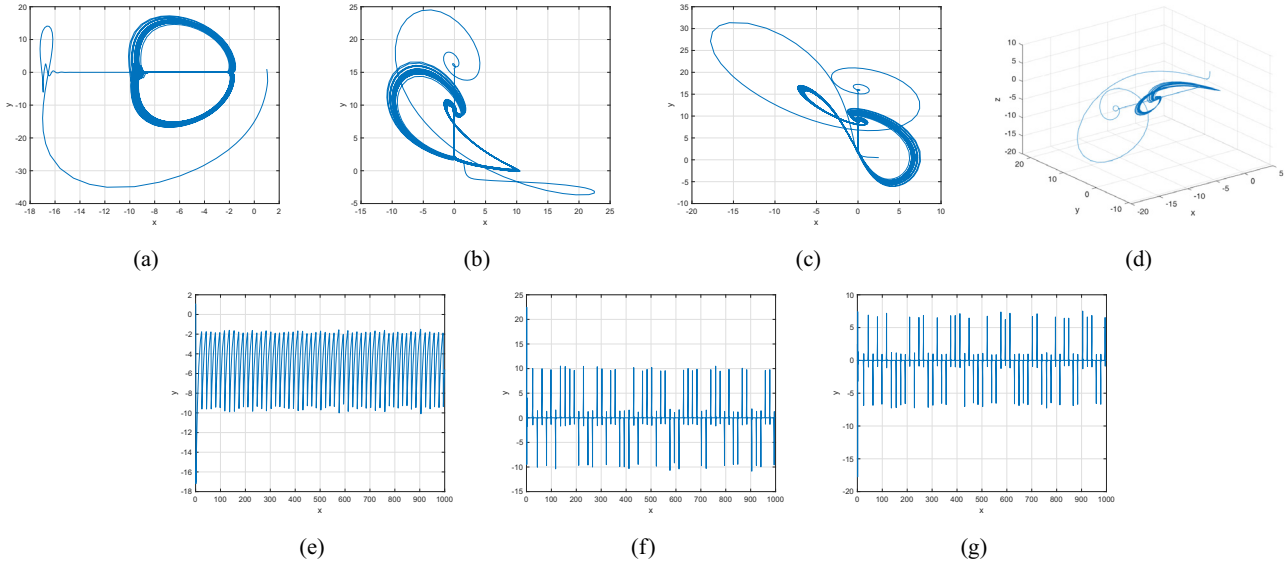

Figure 10: Phase portraits for 2D and 3D discrete fractional spacecraft model (5.1) with fractional-order $\beta(\varpi) = \frac{100 + 99\exp(\varpi/4)}{100(1+\exp(\varpi/4))}$.

5.2 Incommensurate V–O

The interactions of the incommensurate-order discrete fractional spacecraft model are investigated in this part. Incommensurate V–O requires employing distinctive orders to feed every formula in the structure. The incommensurate-order form of discrete fractional spacecraft model is represented in the following manner:

$$\begin{cases} {}^{\mathrm{ABC}}_{\mathbf{d}}\nabla^{\beta_1}_{\varpi}\mathbf{x}_1(\varpi) = \dfrac{1}{3}\mathbf{x}_2(\mathbf{t})\mathbf{x}_3(\mathbf{t}) - \chi_1\mathbf{x}_1(\mathbf{t}) + \dfrac{1}{\sqrt{6}}\mathbf{x}_3(\mathbf{t}), \\ {}^{\mathrm{ABC}}_{\mathbf{d}}\nabla^{\beta_2}_{\varpi}\mathbf{x}_2(\varpi) = -\mathbf{x}_1(\mathbf{t})\mathbf{x}_3(\mathbf{t}) + \chi_2\mathbf{x}_2(\mathbf{t}), \\ {}^{\mathrm{ABC}}_{\mathbf{d}}\nabla^{\beta_3}_{\varpi}\mathbf{x}_3(\varpi) = \mathbf{x}_1(\mathbf{t})\mathbf{x}_2(\mathbf{t}) - \sqrt{6}\,\mathbf{x}_1(\mathbf{t}) - \chi_3\mathbf{x}_3(\mathbf{t}). \end{cases} \tag{5.2}$$

In view of Theorem 4.1, we are able to convey a mathematical representation of the incommensurate-order discrete fractional spacecraft model (5.2) in the following manner:

$$
\begin{cases}
\mathbf{x}_1(\ell) = \mathbf{x}_1(0) + \dfrac{1-\beta_1}{\mathbb{M}(\beta_1)} \\
\left[\dfrac{1}{3}\mathbf{x}_2(\ell)\mathbf{x}_3(\ell) - \chi_1\mathbf{x}_1(\ell) + \dfrac{1}{\sqrt{6}}\mathbf{x}_3(\ell)\right] \\
+ \dfrac{\beta_1}{\mathbb{M}(\beta_1)} \displaystyle\sum_{\kappa=1}^{\ell} \dfrac{\Gamma(\ell-\kappa+\beta_1)}{\Gamma(\ell-\kappa+1)} \\
\left[\dfrac{1}{3}\mathbf{x}_2(\kappa)\mathbf{x}_3(\kappa) - \chi_1\mathbf{x}_1(\kappa) + \dfrac{1}{\sqrt{6}}\mathbf{x}_3(\kappa)\right], \\
\mathbf{x}_2(\ell) = \mathbf{x}_2(0) + \dfrac{1-\beta_2}{\mathbb{M}(\beta_2)}[-\mathbf{x}_1(\ell)\mathbf{x}_3(\ell) + \chi_2\mathbf{x}_2(\ell)] \\
+ \dfrac{\beta_2}{\mathbb{M}(\beta_2)} \displaystyle\sum_{\kappa=1}^{\ell} \dfrac{\Gamma(\ell-\kappa+\beta_2)}{\Gamma(\ell-\kappa+1)}[-\mathbf{x}_1(\kappa)\mathbf{x}_3(\kappa) + \chi_2\mathbf{x}_2(\kappa)], \\
\mathbf{x}_3(\ell) = \mathbf{x}_3(0) + \dfrac{1-\beta_3}{\mathbb{M}(\beta_3)} \\
[\mathbf{x}_1(\ell)\mathbf{x}_2(\ell) - \sqrt{6}\,\mathbf{x}_1(\ell) - \chi_3\mathbf{x}_3(\ell)] \\
+ \dfrac{\beta_3}{\mathbb{M}(\beta_3)} \displaystyle\sum_{\kappa=1}^{\ell} \dfrac{\Gamma(\ell-\kappa+\beta_3)}{\Gamma(\ell-\kappa+1)} \\
[\mathbf{x}_1(\kappa)\mathbf{x}_2(\kappa) - \sqrt{6}\,\mathbf{x}_1(\kappa) - \chi_3\mathbf{x}_3(\kappa)], \\
\mathbb{M}(\beta_\iota) = 1 - \beta_\iota + \dfrac{\beta_\iota}{\Gamma(\beta_\iota)}, \ \iota = 1, 2, 3, \ell \geq 1.
\end{cases} \tag{5.3}
$$

We investigate the processes and distinctive features of this visualization for the purpose of comprehending their peculiar behaviour and investigating the consequences of using distinguished orders in the system's dynamics equations. Figures 12–16 show various chaotic diagrams that show the behaviour of the incommensurate-order discrete fractional spacecraft model (5.3) as the value of $\beta_\iota(\varpi)$ fluctuates between $(0, 1]$. The modelling exercises were performed with the system settings and the ICs $(\mathbf{x}_1(0), \mathbf{x}_2(0), \mathbf{x}_3(0))$ set to $(1.5, 0.5, -0.5)$. These schematics clearly show distinguished trends, pointing out that modifications in V–Os $(\beta_1(\varpi), \beta_2(\varpi), \beta_3(\varpi))$ have an enormous effect on the configurations of the incommensurate-order discrete fractional spacecraft model (5.3). For example, whenever $(\beta_1(\varpi), \beta_2(\varpi), \beta_3(\varpi)) = (1, 0.9, 0.97 + 0.03\tanh(\varpi/10))$, the structure's contends develop *via* repeated to chaotic, using recurring expanding bifurcation when χ_1 improves. However, when $(\beta_1(\varpi), \beta_2(\varpi), \beta_3(\varpi)) = (0.2, 0.97 + 0.03\sin(\varpi/10), 0.8)$, an oscillatory trajectory is noticed, using pathways that stay reliable to earn minimal measurements of χ_1 and transforming into chaos as $\beta_1(\varpi)$ gets closer to 1. In the scenario of $(\beta_1(\varpi), \beta_2(\varpi), \beta_3(\varpi)) = (0.2, 0.2, 0.85)$, a chaotic region is visible all along the range, with the exception of a few

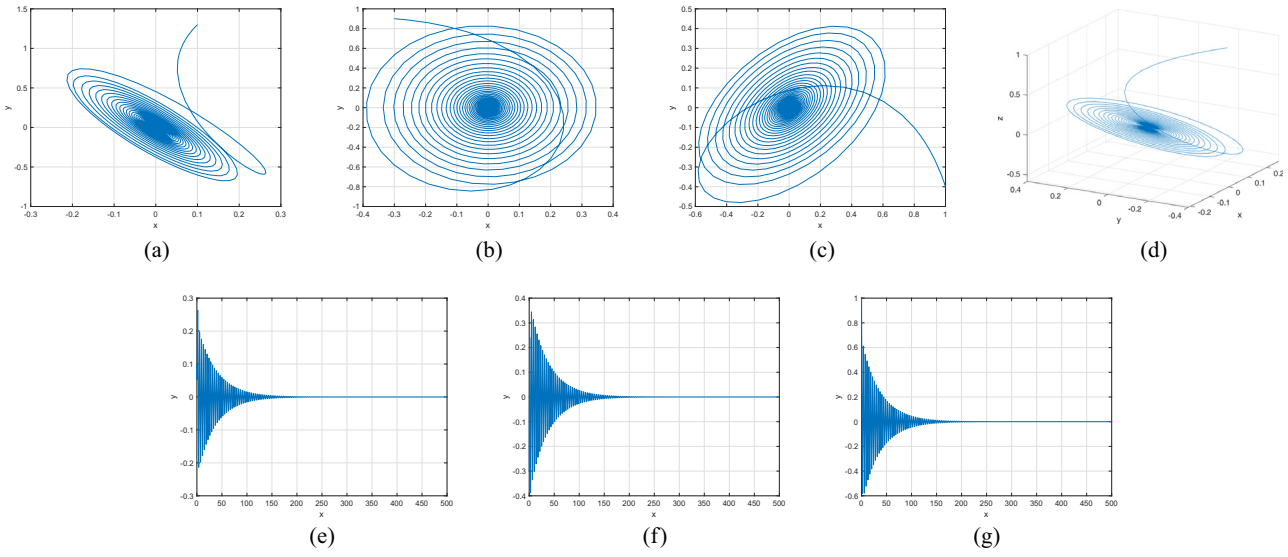

Figure 11: Phase portraits for 2D and 3D discrete fractional spacecraft model (5.1) with V–O $\beta(\varpi) = \frac{1}{100}(97 + 3\cos(\varpi/10))$.

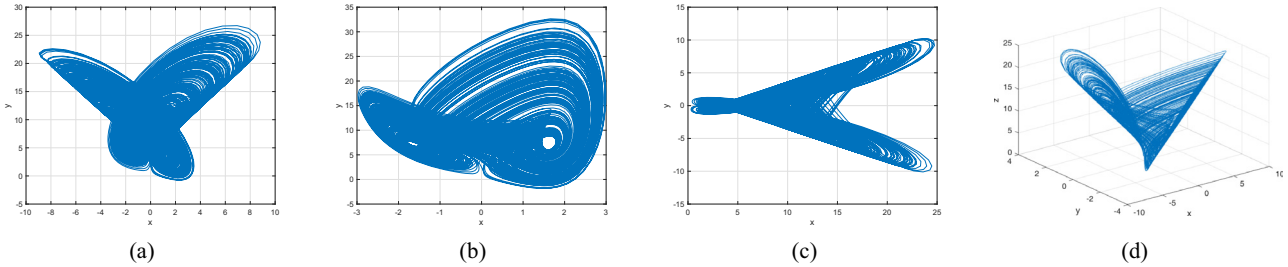

Figure 12: Phase portraits for 2D and 3D for discrete fractional spacecraft model (5.3) with V–O $(\beta_1(\varpi), \beta_2(\varpi), \beta_3(\varpi)) = (1, 0.9, 0.97 + 0.03\tanh(\varpi/10))$.

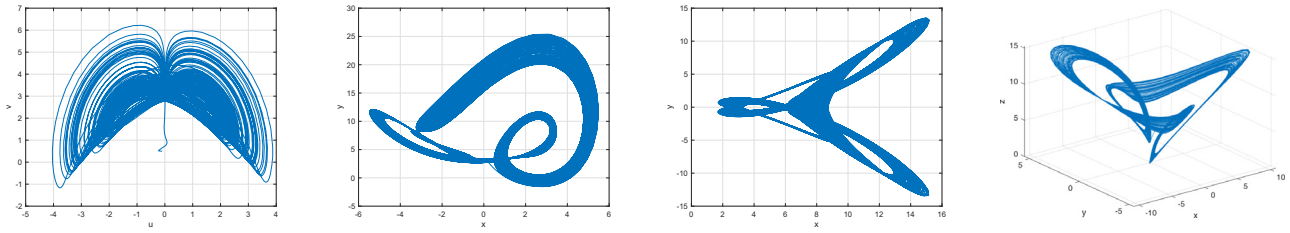

(a) (b) (c) (d)

Figure 13: Phase portraits for 2D and 3D for discrete fractional spacecraft model (5.3) with V–O $(\beta_1(\varpi), \beta_2(\varpi), \beta_3(\varpi)) = (0.2, 0.97 + 0.03\sinh(\varpi/10), 0.8)$.

confined areas where the framework demonstrates frequent fluctuations, particularly as χ_1 decreases towards 0, (Figures 12 and 13). Additional research was additionally performed in three particular situations to offer a more comprehensive example of the impacts of incommensurate orders on the behaviour of the discrete fractional spacecraft model (5.3). Such inquiries provide an improved comprehension of how V–Os affect the functioning of systems and emphasize the significance of taking incommensurate orders into account when analyzing simulation behaviour.

Case I: Figure 14 shows the change with respect to $\beta_1(\varpi)$ *via* 0 to 1 using an incremental dimension of $\Delta\beta_1 = 0.005$. The chaos and associated Poincaré maps of the incommensurate-order discrete fractional spacecraft model (5.3) for $\beta_2(\varpi) = \beta_3(\varpi) = 1 - \cos^2 \varpi/2$ and the system settings with the ICs $(\mathbf{x}_1(0), \mathbf{x}_2(0), \mathbf{x}_3(0))$ set to $(1.5, 0.5, -0.5)$ are shown in these illustrations. Figure 17(a)–(d) shows that the configuration of the incommensurate-order discrete fractional spacecraft model (5.3) demonstrates chaotic behaviour for less extensive variations in $\beta_1(\varpi)$, as indicated in Figure 17(e)–(h). When $\beta_1(\varpi)$ falls within $(0.26, 0.40)$, the Poincaré shown in Figure 17(a)–(d) swings within non-negative and negative regions. Through the appearance of regular apertures, this result suggests the existence of chaotic behaviour. As the incommensurate-order $\beta_1(\varpi)$ expands, paths are transformed from chaotic to consistent movement, which is characterized by orbits that revolve, in which the configurations of

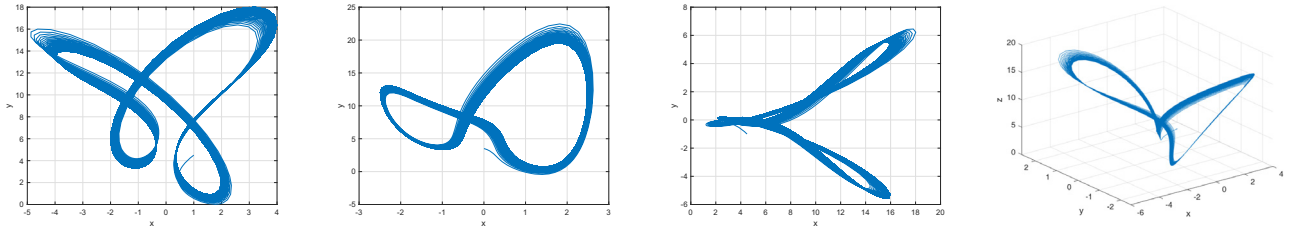

(a) (b) (c) (d)

Figure 14: Phase portraits for 2D and 3D for discrete fractional spacecraft model (5.3) with V–O $(\beta_1(\varpi), \beta_2(\varpi), \beta_3(\varpi)) = (0.65, 1 - \cos^2 \varpi/2, 1 - \cos^2 \varpi/2)$.

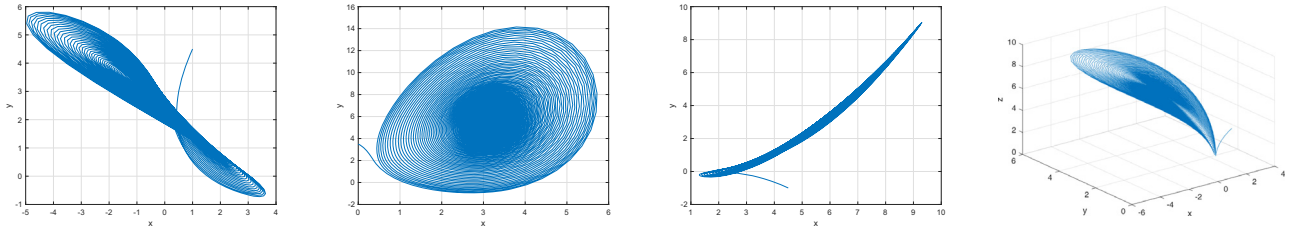

(a) (b) (c) (d)

Figure 15: Phase portraits for 2D and 3D for discrete fractional spacecraft model (5.3) with V–O $(\beta_1(\varpi), \beta_2(\varpi), \beta_3(\varpi)) = (\tanh(\varpi + 1), 0.75, \tanh(\varpi + 1))$.

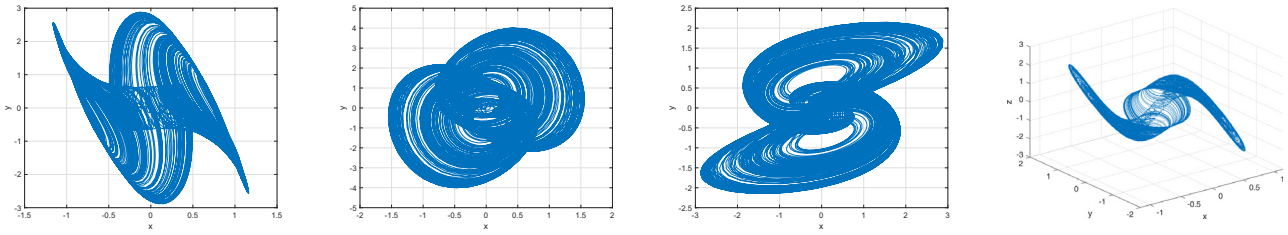

(a) (b) (c) (d)

Figure 16: Phase portraits for 2D and 3D for discrete fractional spacecraft model (5.3) with V–O $(\beta_1(\varpi), \beta_2(\varpi), \beta_3(\varpi)) = (\frac{100 + 90\exp(\varpi/4)}{100(1+\exp(\varpi/4))}, 0.85)$.

the incommensurate-order discrete fractional spacecraft model (5.3) get steady.

Case II: The Poincaré illustrations are displayed for studying the fluctuating behaviours of the incommensurate-order discrete fractional spacecraft model (5.3) *via* $\beta_2(\varpi)$ becoming a configurable factor, as shown in Figures 15(a)–(d) and 17(e)–(h). The modelling steps are carried out by differing $\beta_2(\varpi)$ in the interval $(0, 1)$, whereas maintaining the incommensurate-orders $\beta_1(\varpi) = \beta_3(\varpi) = \tanh(\varpi + 1)$, ICs $(\mathbf{x}_1(0), \mathbf{x}_2(0),$

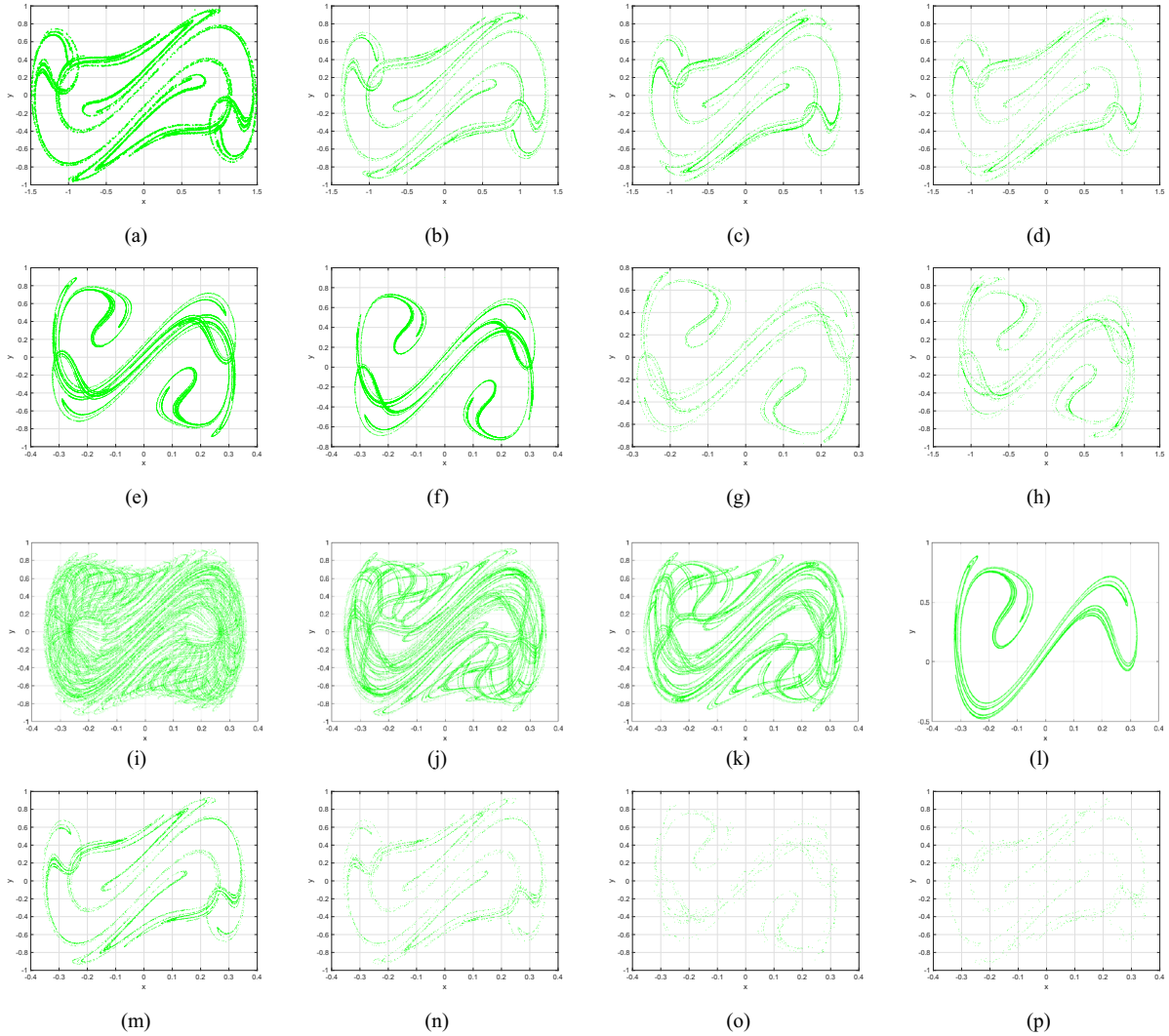

(a) (b) (c) (d)
(e) (f) (g) (h)
(i) (j) (k) (l)
(m) (n) (o) (p)

Figure 17: Poincaré maps for discrete fractional spacecraft model (5.3) for various V–Os as mentioned earlier.

$\mathbf{x}_3(0)) = (1.5, 0.5, -0.5)$, and system settings remains consistent. The illustration shows that while the order $\beta_2(\varpi)$ improves to higher figures, the patterns of motion get less unstable. As $\beta_2(\varpi)$ declines, chaotic practices that have elevated $\Omega_{\max}$ values show up, in addition to the emergence of relatively small regular zones *via* adverse system parameters. Furthermore, as $\beta_2(\varpi)$ falls more thoroughly closer to zero, the chaos pattern fall, after which they come to zero. This is consistent with the appearance of recurring pathways and the evolution of the incommensurate discrete fractional spacecraft model (5.3), regarding chaos to stable decisions. The identified modifications in the poincaré and the accompanying shifting trends demonstrate the mechanism's response to FO $\beta_2(\varpi)$ alternatives, pointing out the intricate nature and adaptability of the incommensurate-order discrete fractional spacecraft model (5.3).

Case III: Figure 16 depicts the chaotic diagram and the accompanying Poincaré map of the identified novel incommensurate-order discrete fractional spacecraft model (5.3) using the parameter $\beta_3(\varpi)$ fluctuated between 0 and 1. We preserve the incommensurate orders as $\beta_1 = \beta_2 = \frac{100 + 90\exp(-\varpi/4)}{100(1+\exp(-\varpi/4))}$ in the present calculation. Figure 16 shows that, in contrast to the earlier instances, the pathways of the incommensurate system reveal chaotic behaviour as the position of $\beta_3(\varpi)$ increases, which is illustrated by greater system parameters. We also observe that as β_3 arrives at 1, the Poincaré map indicates that evolution stipulates and the paths deviate towards infinity, as shown in Figure 17(m)–(p). As an instance, if $\beta_3 = 0.923$ and following a certain quantity of repetitions, particularly χ_3, the pathways deviate towards infinity. As $\beta_3(s)$ decreases, the chaotic decreases likewise, ultimately achieving the lowest possible significance, resulting in less chaotic and, as a result, more predictable interactions of the model's indicates. These findings highlight the incommensurate discrete fractional spacecraft (5.3) responsiveness to fluctuations in order $\beta_3(\varpi)$, which leads to an extensive spectrum of flexible actions involving chaotic and cyclical movements. This emphasizes the importance of incommensurate-orders in determining the behaviour of the framework. Furthermore, as shown in Figure 16, the phase depictions of the configuration factors of the incommensurate discrete fractional spacecraft model (5.3), promote the idea that incommensurate-orders more precisely symbolize the structure's behavioural patterns. To sum up, the research highlights the complex and varied characteristics of the incommensurate-order discrete fractional spacecraft model (5.3), and it also highlights the importance of FO selection in modelling and characterizing its fluctuations.

6 Robust controller model technique

The powerful intolerant fault control system approach to development is explained in the next part. This layout depicts the monitoring plan. The suggested mechanism rules consists of two components:

(A) an insignificant device $\Omega_{\mathcal{N}_1}(\tau + 1 - \beta(\varpi)) = [\Omega_{\mathcal{N}_l}(\tau + 1 - \beta(\varpi))] \in \mathbb{N}_{\mathbf{d}+1}$;

(B) an effective compensation $\Omega_{\mathcal{R}1}(\tau + 1 - \beta(\varpi)) = [\Omega_{\mathcal{R}_l}(\tau + 1 - \beta(\varpi))] \in \mathbb{N}_{\mathbf{d}+1}$.

The insignificant control device is intended in fact for the altered insignificant mechanism; the reliable compensating device is built from second-level filtering to limit the impact of the corresponding interruption. The powerful control device $\Omega(\tau + 1 - \beta(\varpi))$ is then laid out as

$$\begin{aligned}\Omega(\tau + 1 - \beta(\varpi)) = \mathbb{J}_{\mathcal{N}_1}[&\Omega_{\mathcal{N}_1}(\tau + 1 - \beta(\varpi)) \\ &+ \Omega_{\mathcal{R}1}(\tau + 1 - \beta(\varpi))].\end{aligned} \tag{6.1}$$

Let $\omega_\Omega(\tau + 1 - \beta(\varpi)) = [\theta(\tau + 1 - \beta(\varpi))] \in \mathbb{N}_{\mathbf{d}+1}$ represent the time-dependent feedback interruptions. When the spacecraft behaviour monitoring mechanism that experiences parametric fluctuations, outside influences, time-dependent, participation interruptions, motor imperfections, and exhaustion is given as follows:

$$\begin{cases} {}^{\mathrm{ABC}}\nabla_\sigma^{\beta(\varpi)}\varepsilon_{\mathbf{p}_1}(\tau + 1 - \beta(\varpi)) = \varepsilon_\theta(\tau + 1 - \beta(\varpi)), \\ {}^{\mathrm{ABC}}\nabla_\sigma^{\beta(\varpi)}\varepsilon_\theta(\tau + 1 - \beta(\varpi)) \\ = \mathbb{J}_{\mathcal{N}_1}^{-1}\mathfrak{I}(\theta(\tau + 1 - \beta(\varpi)))\mathbb{J}_{\mathcal{N}_1}\theta(\tau + 1 - \beta(\varpi)) \\ - \dot{\theta}(\tau + 1 - \beta(\varpi)) + \mathbb{J}_{\mathcal{N}_1}\Omega(\tau + 1 - \beta(\varpi)) \\ + \mathcal{A}(\tau + 1 - \beta(\varpi)), \end{cases} \tag{6.2}$$

where $\mathbf{p}_1(\tau + 1 - \beta(\varpi))$ signifies the real attitude quaternion and $\mathcal{A}(\tau + 1 - \beta(\varpi)) = [\mathcal{A}_\iota(\tau + 1 - \beta(\varpi))] \in \mathbb{N}_{\mathbf{d}} + 1$ represents the structure's analogous disruption provided as follows:

$$\begin{aligned}&\mathcal{A}(\tau + 1 - \beta(\varpi)) \\ &= \begin{cases} \mathbb{J}_{\mathcal{N}_1}^{-1}\mathfrak{I}(\theta(\tau + 1 - \beta(\varpi)))\mathbb{J}_{\mathcal{N}_1}\theta(\tau + 1 - \beta(\varpi)) \\ -\mathbb{J}_{\mathcal{N}_1}^{-1}\mathfrak{I}(\theta(\tau + 1 - \beta(\varpi)))\mathbb{J}\Omega(\tau + 1 - \beta(\varpi)) \\ +\mathbb{J}^{-1}\mathbf{d}(\tau + 1 - \beta(\varpi)) + \mathbb{J}_{\mathcal{N}_1}^{-1}\Omega(\tau + 1 - \beta(\varpi)) \\ +\mathbb{J}^{-1}[\hbar(\tau + 1 - \beta(\varpi) - \omega_\Omega(\tau + 1 - \beta(\varpi))) \\ \times\Omega(\tau + 1 - \beta(\varpi) - \omega_\Omega(\tau + 1 - \beta(\varpi))) + \Omega(\tau \\ \quad + 1 - \beta(\varpi) - \omega_\Omega(\tau + 1 - \beta(\varpi)))]. \end{cases}\end{aligned}$$

Considering (6.1) and (6.2), then the spacecraft dynamic framework is subsequently expressed as follows:

$$
\begin{aligned}
&{}^{\mathrm{ABC}}\nabla_{\sigma}^{\beta(\varpi)}\varepsilon_{\mathbf{p}_1}(\tau+1-\beta(\varpi))\\
&\quad=\ -\mathbb{J}_{\mathcal{N}_1}^{-1}\mathfrak{I}(\theta(\tau+1-\beta(\varpi)))\mathbb{J}_{\mathcal{N}_1}\theta(\tau+1-\beta(\varpi))\\
&\qquad+\dot{\theta}(\tau+1-\beta(\varpi))\\
&\qquad+\Omega_{\mathcal{N}_1}(\tau+1-\beta(\varpi))+\Omega_{\mathcal{R}1}(\tau+1-\beta(\varpi))\\
&\qquad+\mathcal{A}(\tau+1-\beta(\varpi)).
\end{aligned}
\tag{6.3}
$$

Then, in (6.3), the perturbation-free insignificant mechanism can be retrieved mechanically by overlooking the reliable a compensator $\Omega_{\mathcal{R}1}(\tau+1-\beta(\varpi))$ and corresponding disruption $\mathcal{A}(\tau+1-\beta(\varpi))$. The insignificant device can be constructed with precise simulation data as follows:

$$
\begin{aligned}
&\Omega_{\mathcal{N}_1}(\tau+1-\beta(\varpi))\\
&\quad=\ -\Psi_{\theta}\varepsilon_{\theta}(\tau+1-\beta(\varpi))-\Psi_{\mathbf{p}_1}\varepsilon_{\mathbf{p}_1}(\tau+1-\beta(\varpi))\\
&\qquad+\mathbb{J}_{\mathcal{N}_1}^{-1}\mathfrak{I}(\theta\Psi_{\theta}\varepsilon_{\theta}(\tau+1-\beta(\varpi)))\\
&\qquad\times\mathbb{J}_{\mathcal{N}_1}\theta(\tau+1-\beta(\varpi))+\dot{\theta}(\tau+1-\beta(\varpi)),
\end{aligned}
\tag{6.4}
$$

where the matrices $\Psi_{\theta}=\mathrm{diag}(\Xi_{\theta_{\mathbf{x}_1}},\Xi_{\theta_{\mathbf{x}_2}},\Xi_{\theta_{\mathbf{x}_3}})$ are control device acquires and $\Psi_{\mathbf{p}_1}=\mathrm{diag}(\Xi_{\mathbf{p}_1},\Xi_{\mathbf{p}_2},\Xi_{\mathbf{p}_3})$ are non-negative constants to be identified.

In addition, the effective compensated $\Omega(\tau+1-\beta(\varpi))$ is anticipated to entirely limit the corresponding disruption $\mathcal{A}(\tau+1-\beta(\varpi))$. A reliable compensating device in the intricate frequency spectrum is able to be constructed with a second-order filtrate $\mathcal{G}(\varpi)$ as follows:

$$
\Omega_{\mathcal{R}1}(\varpi)=-\mathcal{G}(\varpi)\mathcal{A}(\varpi),
\tag{6.5}
$$

where ϖ indicates the Laplace operator and $\mathcal{G}(\mathbf{s}_1)=\mathrm{diag}(\mathcal{G}_1(\mathbf{s}_1),\mathcal{G}_2(\mathbf{s}_1),\mathcal{G}_3(\mathbf{s}_1))$. Nevertheless, measuring an analogous disruption $\mathcal{A}(\mathbf{s}_1)$ in practise figuring is challenging. As a result, the Laplace inverse transformation of (6.5) fails to generate the reliable compensating device $\Omega_{\mathcal{R}1}(\tau+1-\beta(\varpi))$.

In consideration of this, the researchers determine to interpret the analogous disruption $\mathcal{A}(\tau+1-\beta(\varpi))$ as a tampering of the perspective measuring angular momentum. The analogous interference $\Omega_{\mathcal{R}1}(\tau+1-\beta(\varpi))$ is subsequently provided by (6.3) as follows:

$$
\begin{aligned}
\mathcal{A}(\tau+1-\beta(\varpi))=\ &{}^{\mathrm{ABC}}\nabla_{\sigma}^{\beta(\varpi)}(\tau+1-\beta(\varpi))\varepsilon_{\mathbf{p}_1}(\tau+1-\beta(\varpi))\\
&+\mathbb{J}_{\mathcal{N}_1}^{-1}\mathfrak{I}(\theta(\tau+1-\beta(\varpi)))\\
&\times\mathbb{J}_{\mathcal{N}_1}\theta(\tau+1-\beta(\varpi))\\
&+\dot{\theta}(\tau+1-\beta(\varpi))-\mathbb{J}_{\mathcal{N}_1}^{-1}\Omega(\tau+1-\beta(\varpi)).
\end{aligned}
\tag{6.6}
$$

In view of (6.5) and (6.6), the sturdy compensating device $\Omega_{\mathcal{R}1}(\tau+1-\beta(\varpi))$, $\tilde{L}(\tau+1-\beta(\varpi))=\mathbb{J}_{\mathcal{N}_1}^{-1}\mathfrak{I}(\theta(\tau+1-\beta(\varpi)))\mathbb{J}_{\mathcal{N}_1}\theta(\tau+1-\beta(\varpi))+\dot{\theta}(\tau+1-\beta(\varpi))$ and $\mathbf{L}(\varpi)$ represent its Laplace transformation. The corresponding interference $\mathcal{A}(\mathbf{s}_1)$ is then able to composed as follows:

$$
\mathcal{A}(\mathbf{s}_1)=\mathbf{s}_1^2\varepsilon_{\mathbf{p}_1}(\varpi)+\mathbf{L}(\mathbf{s}_1)-\mathbb{J}_{\mathcal{N}_1}^{-1}\Omega(\mathbf{s}_1).
\tag{6.7}
$$

Plugging (6.5) into (6.7), then the powerful devise can be expressed as follows:

$$
\Omega_{\mathcal{R}1}(\mathbf{s}_1)=\mathcal{G}^2[\mathfrak{r}_2(\mathbf{s}_1)-\varepsilon_{\mathbf{p}_1}(\mathbf{s}_1)],
\tag{6.8}
$$

where $\mathfrak{r}_2(\mathbf{s}_1)=(\mathbf{s}_1+\mathfrak{I}\mathcal{G})^{-2}[\mathbb{J}_{\mathcal{N}_1}^{-1}\Omega(\mathbf{s}_1)-\mathbf{L}(\mathbf{s}_1)+(2\mathbf{s}_1\mathcal{G}+\mathcal{G}^2)\varepsilon_{\mathbf{p}_1}(\mathbf{s}_1)]$.

After simplification, we have

$$
\begin{aligned}
\Omega_{\mathcal{R}1}(\tau+1-\beta(\varpi))=\mathcal{G}^2[&\mathfrak{r}_2(\tau+1-\beta(\varpi))\\
&-\varepsilon_{\mathbf{p}_1}(\tau+1-\beta(\varpi))].
\end{aligned}
\tag{6.9}
$$

Multiplying $\mathfrak{r}_2(\mathbf{s}_1)$ by $(\mathbf{s}_1\mathfrak{I}+\mathcal{G})$, then we can find

$$
\begin{aligned}
{}^{\mathrm{ABC}}\nabla_{\sigma}^{\beta(\varpi)}\mathfrak{r}_2(\tau+1-\beta(\varpi))=&-\mathcal{G}\mathfrak{r}_2(\tau+1-\beta(\varpi))\\
&+2\mathcal{G}\varepsilon_{\mathbf{p}_1}(\tau+1-\beta(\varpi))\\
&+\phi(\tau+1-\beta(\varpi)).
\end{aligned}
\tag{6.10}
$$

Analogously, we can find

$$
\begin{aligned}
&{}^{\mathrm{ABC}}\nabla_{\sigma}^{\beta(\varpi)}\phi(\tau+1-\beta(\varpi))\\
&\quad=\ -\mathcal{G}\phi(\tau+1-\beta(\varpi))-\mathcal{G}\varepsilon_{\mathbf{p}_1}(\tau+1-\beta(\varpi))\\
&\qquad+\mathbb{J}_{\mathcal{N}_1}^{-1}\Omega(\tau+1-\beta(\varpi))\\
&\qquad-\mathbb{J}_{\mathcal{N}_1}^{-1}\mathfrak{I}(\theta(\tau+1-\beta(\varpi)))\mathbb{J}_{\mathcal{N}_1}(\tau+1-\beta(\varpi))\\
&\qquad-\dot{\theta}(\tau+1-\beta(\varpi)),
\end{aligned}
\tag{6.11}
$$

where $\phi(\tau+1-\beta(\varpi))$, $\mathfrak{r}_2(\tau+1-\beta(\varpi))\in\mathbb{N}_{\mathbf{d}+1}$ presents compensating device states and $\mathcal{G}=\mathrm{diag}(\hbar_1,\hbar_2,\hbar_3)$ is a diagonal constant matrix containing compensating device factors. It is clear that the setting $\mathcal{G}$ has a major effect on both compensation generates and the reliability of the compensation state spaces. The suggested sturdy device ut can subsequently be calculated using (6.1), (6.4), (6.10), and (6.11).

In addition, the following is the recommendations for determining the theoretical controller boosts Ψ_{θ} and $\Psi_{\mathbf{p}_1}$ and the compensatory value $\mathcal{G}$:

Case I: Take out the disturbance-free insignificant structure using (6.3), and then choose the default controller's advantages Ψ_{θ} and $\Psi_{\mathbf{p}_1}$ to achieve the envisioned effectiveness.

Case II: Choose an effective compensating device parameter specification $\mathcal{G}$ is large enough. In broad terms, the tightly controlled system's influence preciseness can be substantially enhanced.

Case III: In view of control assumption, the regulation precisioness condition issatisfied, the regulation preciseness prerequisite, the sturdy a compensator value $\mathcal{G}$ can be decreased to an adequate figure for preserving power.

Case IV: When the envisioned regulate exactness is unable to be obtained by simply adjusting the compensating setting $\mathcal{G}$, it is suggested to revert to **Case I**, choose wider insignificant controller acquires Ψ_θ and $\Psi_{\mathbf{p}_1}$ and subsequently continue to **Cases 2** and **3**.

Remark 6.1. It is noted that the mechanism suggested in (6.1) does not necessitate any details about device error. Furthermore, the intended improvement of the mechanism Ψ_θ and $\Psi_{\mathbf{p}_1}$ and the compensator factor $\mathcal{G}$ are correspondingly non-negative constant matrices. As a result, the suggested controller structure is straightforward and time independent. These characteristics are desired in realistic engineering.

Remark 6.2. The insignificant framework can be streamlined using the nominative influence rules in (6.4) as ${}^{\mathrm{ABC}}\nabla_\sigma^{\beta(\varpi)}\varepsilon_{\mathbf{p}_1}(\tau+1-\beta(\varpi)) + \Psi_\theta\varepsilon_{\mathbf{p}_1}(\tau+1-\beta(\varpi)) + \Psi_{\mathbf{p}_1}\varepsilon_{\mathbf{p}_1}(\tau+1-\beta(\varpi)) = 0$. It eventually becomes a standard proportional-derivative regulate framework. Evidently, if insignificant controller improvements $\Psi_{\mathbf{p}_1}$ and Ψ_θ are chosen with appropriate figures, the poles of the insignificant framework can be assigned to any anticipated amount.

In addition, the genuine mechanism results $\Omega(\tau+1-\beta(\varpi))$ show several unpredictability issues involving feedback interruptions, mechanism exhaustion, and supplementary breakdowns. Higher compensating device factors also result in an increasingly significant saturation level challenge. This makes sense considering that greater compensating device settings result in deeper compensation forces. Furthermore, when viewed alongside $\mathcal{G}$ situations, the monitoring system in [85] hinders saturation by implementing an arc connection function as $\mathcal{F}_1(\Omega)$. Following that, at first, the actual mechanism results decreased due to the influence of matrix Ψ_θ. Similarly, the mechanism's use of energy is examined. As illustrated in Figure 18(a)–(b), the structure, *via* wider compensatory factors, devours more power. The electrical system's vitality, on the other hand, is essential but scarce for spacecraft. As a result, if the intended position regulates preciseness, there is no requirement to choose compensating device factors that are excessively large. At this point, regardless of the situation, power intake in the secure phases is concluded. In the meantime, when viewed alongside $\beta(\varpi)$, the processor's results increase in the secure stage considering the equilibrium oversight in the sinusoidal waveform monitoring scenario is greater. This behaviour is mirrored in the equilibrium power use as well as the time reaction demonstrated in Figure 19.

6.1 Synchronization

Nonlinear regulators for coordinating the fractional-order spacecraft model are described in the subsequent section. The synchronization procedure seeks to minimize the difference between the master and slave visualizations, which compels it to gravitate towards zero. The master system is the commensurate fractional-order spacecraft model, represented by (5.1), while the slave system is characterized in the following manner:

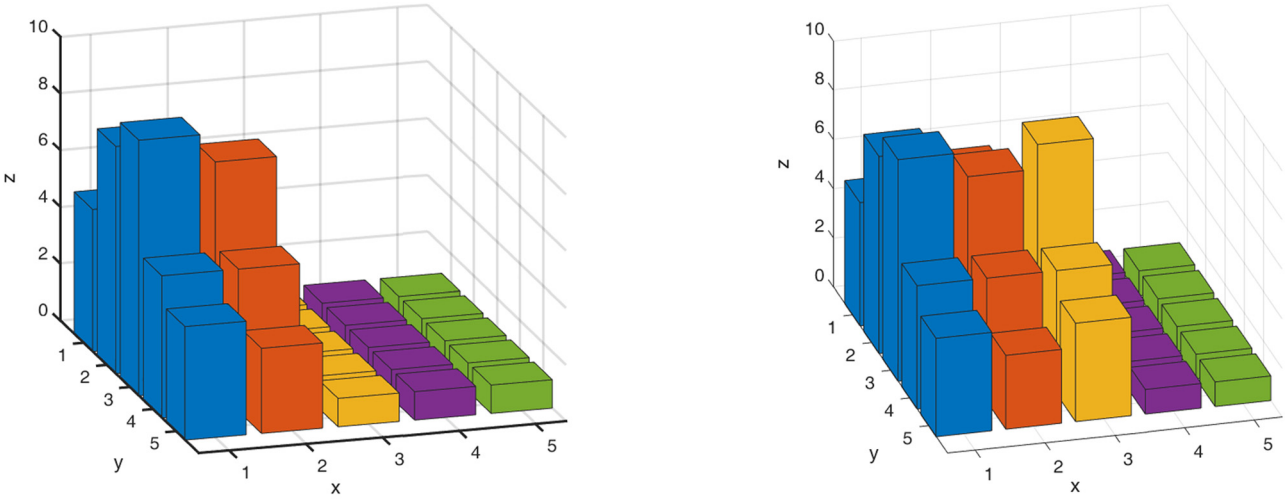

Figure 18: Bar graph containing energy factors and fractional order $\beta(\varpi) = 1$.

$$\begin{cases} {}^{\mathrm{ABC}}_{\mathbf{d}}\nabla^{\beta(\varpi)}_{\varpi}\mathbf{x}_{1\mathbf{n}}(\tau) \\ \quad = \dfrac{1}{3}\mathbf{x}_{2\mathbf{n}}(\ell)\mathbf{x}_{3\mathbf{n}}(\ell) \\ \quad - \mathbf{d}\mathbf{x}_{1\mathbf{n}}(\ell) + \dfrac{1}{\sqrt{6}}\mathbf{x}_{3\mathbf{n}}(\ell) - \mathbf{x}_{1\mathbf{n}}(\ell) + \mathcal{V}_1(\ell), \\ {}^{\mathrm{ABC}}_{\mathbf{d}}\nabla^{\beta(\varpi)}_{\varpi}\mathbf{x}_{2\mathbf{n}}(\tau) \\ \quad = -\mathbf{x}_{1\mathbf{n}}(\ell)\mathbf{x}_{3\mathbf{n}}(\ell) \\ \quad + b_1\mathbf{x}_{2\mathbf{n}}(\ell) - \mathbf{x}_{2\mathbf{n}}(\ell) + \mathcal{V}_2(\ell), \\ {}^{\mathrm{ABC}}_{\mathbf{d}}\nabla^{\beta(\varpi)}_{\varpi}\mathbf{x}_{3\mathbf{n}}(\tau) \\ \quad = \mathbf{x}_{1\mathbf{n}}(\ell)\mathbf{x}_{3\mathbf{n}}(\ell) \\ \quad - \sqrt{6}\,\mathbf{x}_{1\mathbf{n}}(\ell) - \mathbf{c}\mathbf{x}_{3\mathbf{n}}(\ell) + \mathcal{V}_3(\ell), \end{cases} \tag{6.12}$$

where $\mathcal{V}_1, \mathcal{V}_2$, and $\mathcal{V}_3$ indicate the synchronization regulators.

The fractional error scheme is described as follows:

$$\begin{cases} {}^{\mathrm{ABC}}_{\mathbf{d}}\nabla^{\beta(\varpi)}_{\varpi}\varepsilon_1(\tau) \\ \quad = \left(\dfrac{1}{3}\mathbf{x}_{2\mathbf{n}}(\ell)\mathbf{x}_{3\mathbf{n}}(\ell) - \mathbf{d}\mathbf{x}_{1\mathbf{n}}(\ell) + \dfrac{1}{\sqrt{6}}\mathbf{x}_{3\mathbf{n}}(\ell) \right. \\ \quad \left. + \mathcal{V}_1(\ell)\right) \\ \quad - \left(\dfrac{1}{3}\mathbf{x}_2(\ell)\mathbf{x}_3(\ell) - \mathbf{d}\mathbf{x}_1(\ell) + \dfrac{1}{\sqrt{6}}\mathbf{x}_3(\ell)\right) - \varepsilon_1(\ell), \\ {}^{\mathrm{ABC}}_{\mathbf{d}}\nabla^{\beta(\varpi)}_{\varpi}\varepsilon_2(\tau) \\ \quad = (-\mathbf{x}_{1\mathbf{n}}(\ell)\mathbf{x}_{3\mathbf{n}}(\ell) + b_1\mathbf{x}_{2\mathbf{n}}(\ell) + \mathcal{V}_2(\ell)) \\ \quad - (-\mathbf{x}_1(\ell)\mathbf{x}_3(\ell) + b_1\mathbf{x}_2(\ell)) - \varepsilon_2(\ell), \\ {}^{\mathrm{ABC}}_{\mathbf{d}}\nabla^{\beta(\varpi)}_{\varpi}\varepsilon_3(\tau) \\ \quad = (\mathbf{x}_{1\mathbf{n}}(\ell)\mathbf{x}_{3\mathbf{n}}(\ell) - \sqrt{6}\,\mathbf{x}_{1\mathbf{n}}(\ell) - \mathbf{c}\mathbf{x}_{3\mathbf{n}}(\ell) \\ \quad + \mathcal{V}_3(\ell)) \\ \quad - (\mathbf{x}_1(\ell)\mathbf{x}_3(\ell) - \sqrt{6}\,\mathbf{x}_1(\ell) - \mathbf{c}\mathbf{x}_3(\ell)) - \varepsilon_3(\ell), \end{cases} \tag{6.13}$$

The suggested regulation govern that creates this synchronization system is described in the following theorem.

Theorem 6.1. *Under the supposition of* (6.12) *and* (6.13):

$$\begin{cases} \mathcal{V}_1(\ell) = -\dfrac{1}{3}(\mathbf{x}_{2\mathbf{n}}(\ell)\mathbf{x}_{3\mathbf{n}}(\ell) - \mathbf{x}_2(\ell)\mathbf{x}_3(\ell)) \\ \quad + \mathbf{d}(\mathbf{x}_{1\mathbf{n}}(\ell) - \mathbf{x}_1(\ell)) - \dfrac{1}{\sqrt{6}}(\mathbf{x}_{3\mathbf{n}}(\ell) - \mathbf{x}_3(\ell)), \\ \mathcal{V}_2(\ell) = (\mathbf{x}_{1\mathbf{n}}(\ell)\mathbf{x}_{3\mathbf{n}}(\ell) - \mathbf{x}_1(\ell)\mathbf{x}_3(\ell)) \\ \quad - b_1(\mathbf{x}_{2\mathbf{n}}(\ell) - \mathbf{x}_2(\ell)) - \beta_2\varepsilon_2(\ell), \\ \mathcal{V}_3(\ell) = -(\mathbf{x}_{1\mathbf{n}}(\ell)\mathbf{x}_{3\mathbf{n}}(\ell) - \mathbf{x}_1(\ell)\mathbf{x}_3(\ell)) \\ \quad + \sqrt{6}\,(\mathbf{x}_{1\mathbf{n}}(\ell) - \mathbf{x}_1(\ell)) + \mathbf{c}(\mathbf{x}_{3\mathbf{n}}(\ell) - \mathbf{x}_3(\ell)) \\ \quad - \beta_3\varepsilon_3(\ell), \end{cases} \tag{6.14}$$

where $\beta_2 \in (-1, 2^{\beta} - 1)$ *and* $\beta_3 \in (0, 2^{\beta})$. *Then, the master spacecraft model* (5.1) *and slave spacecraft model* (6.12) *are synchronized.*

Proof. Plugging the regulate principle (6.16) in the fractional error system (6.13), we find:

$$\begin{aligned} &{}^{\mathrm{ABC}}_{\mathbf{d}}\nabla^{\beta(\varpi)}_{\varpi}(\varepsilon_1(\tau), \varepsilon_2(\tau), \varepsilon_3(\tau))^{\mathbf{T}} \\ &\quad = \Phi \times (\varepsilon_1(\tau), \varepsilon_2(\tau), \varepsilon_3(\tau))^{\mathbf{T}}, \end{aligned} \tag{6.15}$$

where

$$\Phi = \begin{pmatrix} -(1+\chi_1) & 0 & 0 \\ 0 & -(1+\beta_2) & 0 \\ 0 & 0 & -\beta_3 \end{pmatrix}. \tag{6.16}$$

Since $\omega_1 = -(1+\chi_1)$, $\omega_2 = -(1+\beta_2)$ and $\omega_3 = -\beta_3$ are the eigenvalues of (6.16). Thus, $\omega_\iota, \iota = 1, 2, 3$ comply with the stability the requirement mentioned in Theorem 2.1 for

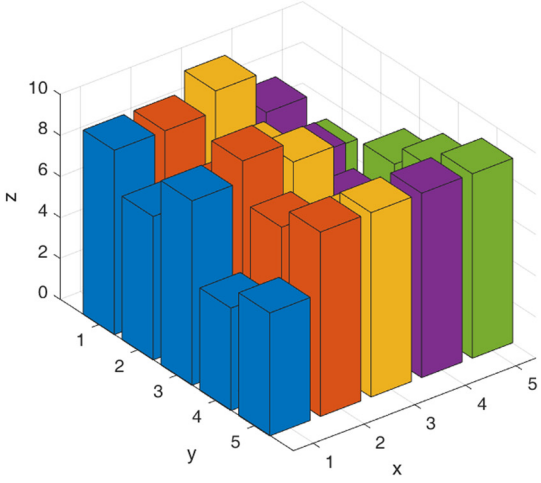

(a)

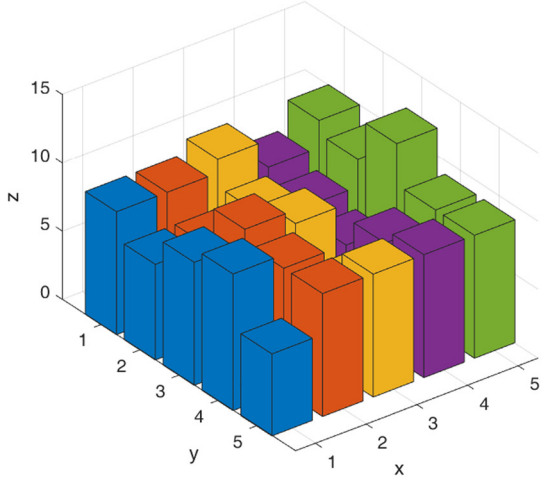

(b)

Figure 19: Bar graph containing energy factors and fractional order $\beta(\varpi) = 0.96$.

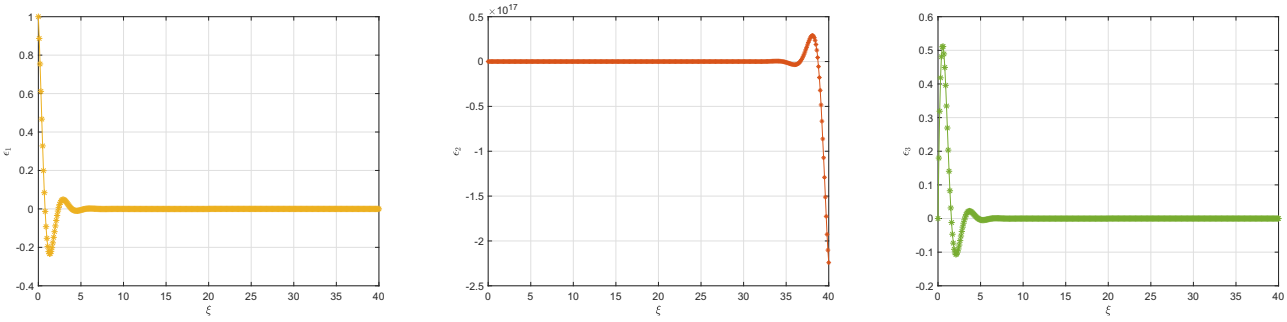

Figure 20: Error dynamics of (5.1) having $(\varepsilon_1, \varepsilon_2, \varepsilon_3) = (1.0, 1.0, 1.0)$.

$\beta_2 \in (-1, 2^{\beta} - 1)$ and $\beta_3 \in (0, 2^{\beta})$, illustrating that the zero outcome of the fractional error model (6.12) is asymptotically stable, resulting in the synchronization of the master spacecraft model (5.1) and the slave spacecraft model (6.12). □

Mathematical computations using MATLAB are used to verify the truthfulness of this outcome. The parameters used are $\chi_1 = 0.4, \chi_2 = 0.175, \chi_3 = 0.4$ and the initial settings are $(\varepsilon_1(0), \varepsilon_2(0), \varepsilon_3(0)) = (1.0, 1.0, -1.0)$. Figure 20(a)–(c) depicts the time formation of the fractional error model's contends (6.12). The graph unambiguously shows that erroneous values are often zero, affirming the efficacy of the previously addressed synchronization technique.

7 Conclusion

The spacecraft interacts with the plasma physics such as solar wind, magnetospheres, and ionospheres. Understanding plasma physics helps mitigate effects like spacecraft charging and drag in low-earth orbit. This article proposes a discrete fractional spacecraft model and investigates its behaviour with commensurate and incommensurate V–Os. The Poincaré map's assessment revealed a variety of unpredictable features, pointing out its dynamic diversity. The distinguished behaviours of the identified discrete fractional spacecraft model have been studied for both commensurate and incommensurate V–Os using various approaches to inspection, including phase pictures and time-evolution plots. Furthermore, the system's challenges have been determined employing the robust controller technique with the actuator faults. The results highlight the significant impact of the network setting and fractional exponents on the configurations of the discrete fractional spacecraft model. The numerical representations of such variables are crucial for influencing the structure and functioning of the framework, and fluctuations in their significance result in various paths as well as effects in the system's state domain. Finally, the article suggests efficient oversight rules for ensuring the reliability and synchronization of the implemented system by manipulating its status to asynchronously tend to zero. The numerical analyses performed provide an extensive overview of the mechanism's interactions and illustrate its fascinating and distinct behaviours, which have been crucial in investigating the consequences of fractional spacecraft models.

In the future, the emergency network will evolve in the patterns of intelligence, integration, popularization, inexpensiveness, and space–air–ground–sea integration. Thanks to the continual growth of finances and societies as a whole, the emergency communication network has been additionally enhanced, and novel technologies for networks have come into existence. This will help expedite the commencement of emergency rescue operations.

Funding information: The author states no funding involved.

Author contribution: The author has accepted responsibility for the entire content of this manuscript and approved its submission.

Conflict of interest: The author states no conflict of interest.

Data availability statement: Data sharing is not applicable to this article as no datasets were generated or analysed during the current study.

References

[1] Carroll TL, Pecora LM, Synchronization chaotic circuits. IEEE Trans CAS. 1999;I(38):435–46.

[2] Pecora LM, Carroll TL. Synchronization in chaotic systems. Phys Rev Lett. 1990:64;821–4.

[3] Djaouida S. Synchronization of a perturbed spacecraft attitude motion. Int J Mech Aerosp Ind Mechatron. Manuf Eng. 2014;8(4):734–8.
[4] Guan P, Liu XJ, Liu JZ. Flexible spacecraft attitude control via sliding mode technique. In: Proceedings of the 44th IEEE Conference on Decision and Control, and the European Control Conference 2005 Seville, Spain. 12–15 Dec, 2005.
[5] Smale S. Differentiable dynamical systems. Bull Am Math Soc. 1967:73;747–817.
[6] Wang YW, Guan ZH, Wen X. Adaptive synchronization for Chen chaotic system with fully unknown parameters. Chaos Solit Fract. 2004;19:899–903.
[7] Lin JS, Liao TL, Yan JJ, Yau HT. Synchronization of unidirectional coupled chaotic systems with unknown channel time-delay: adaptive robust observer-based approach. Chaos Solit Fract. 2005:26(3):971–8.
[8] Fan Y, Wang W, Lin Y. Synchronization of a class of chaotic systems based on adaptive control design of input-to-state stability. Int J Innov Comput Inf Cont. 2015:11(3):803–14.
[9] Chen M, Luo X, Suo Y, Xu Q, Wu H. Hidden extreme multistability and synchronicity of memristor-coupled non-autonomous memristive Fitzhugh-Nagumo models. Nonlin Dyn. 2023;111:7773–88. doi: https://doi.org/10.1007/s11071-023-08235-x.
[10] Duan GR, Yu HH. LMI in control systems analysis, design and applications. Boca Raton: CRC Press; 2013.
[11] Hamidzadeh SM, Esmaelzadeh R. Control and synchronization chaotic spacecraft using active control. Int J Comp Appl. 2014;94(10).
[12] Tuai AP, Jones AJ, The control of higher dimensional chaos: comparative results for the chaotic spacecraft attitude control problem. Phys Nonlin Phenom. 2000;135(1–2):41–62.
[13] Wei W, Wang J, Zuo M, Liu Z, Du J. Chaotic spacecraft attitude control by adaptive approach, Int. J. Control. 2014;87(6):1196–207.
[14] Köose E. Controller design by using non-linear control methods for spacecraft chaotic system. Electr Eng. 2017;99(2):763–73.
[15] Faramin M, Ataei M. Chaotic attitude analysis of a spacecraft via Lyapunov exponents and its robust nonlinear control subject to disturbances and uncertainties, Nonlin Dyn. 2016;83(1–2):361–74.
[16] Farid Y, Moghaddam TV. Generalized projective synchronization of chaotic spacecrafts problem using linear matrix inequality. Int J Dyn Cont. 2014;2(4):577–86.
[17] Du H, Li S. Attitude synchronization for flexible spacecraft with communication delays. IEEE Trans Automat Cont. 2016;61(11):3625–30.
[18] Wu B, Wang D, Poh EK. Decentralized robust adaptive control for attitude synchronization under directed communication topology. J Guid Cont Dyn. 2011;34(4):1276–82.
[19] Zhou N, Xia Y, Wang M, Fu M. Finite-time attitude control of multiple rigid spacecraft using terminal sliding mode. Int J Robust Nonlin Cont. 2015;25(12):1862–76.
[20] MacKunis W, Dupree K, Bhasin S, Dixon WE. Adaptive neural network spacecraft attitude control in the presence of inertia and CMG actuator uncertainties. in: 2008 American Control Conference IEEE. 2008. p. 2975–80.
[21] Show LL, Juang JC, Jan YW. An LMI-based nonlinear attitude control approach. IEEE Trans Cont Sys Tech. 2003;11(1):73–83.
[22] Zhang C, Chen Z, Wei C. Sliding mode disturbance observer-based backstepping control for a transport aircraft, Sci China Inf Sci. 2014;57(5):1–16.
[23] Li HY, Hu YA. Robust sliding-mode backstepping design for synchronization control of cross-strict feedback hyperchaotic systems with unmatched uncertainties. Commun Nonl Sci Numer Sim. 2011;16(10):3904–13.
[24] Cong B, Liu X, Chen Z. Backstepping based adaptive sliding mode control for spacecraft attitude maneuvers, Aero Sci Tech. 2013;30(1):1–7.
[25] Hilfer R, Applications of fractional calculus in physics. Singapore: World Scientific; 2000.
[26] Atici FM, Eloe P. Discrete fractional calculus with the nabla operator. Electron J Qual Theory Differ Equ. 2009;3:2009.
[27] Anastassiou GA. Principles of delta fractional calculus on time scales and inequalities. Math Comput Mode. 2010;52:556–66.
[28] Chu YM, Alzahrani T, Rashid S, Alhulayyil H, Rashidah W, Rehman S. Complex dynamical analysis of fractional differences Willamowski-Rössler chemical reaction model in time-scale analysis, Res Phy. 2023;54(6):107023.
[29] Xu C, Farman M. Qualitative and ulam-Hyres stability analysis of fractional order cancer-immune model. Chaos Solit Fract. 2023:177;114277.
[30] Chu YM, Alzahrani T, Rashid S, Rashidah W, Rehman S, Alkhatib M. An advanced approach for the electrical responses of discrete fractional-order biophysical neural network models and their dynamical responses. Sci Rep. 2023;13(1).
[31] Farman M, Shehzad A, Nisar KS, Hincal E, Akgúl A, Hassan AM. Generalized Ulam-Hyers-Rassias stability and novel sustainable techniques for dynamical analysis of global warming impact on ecosystem. Sci Reports. 2023;13:22441.
[32] Gafel HS, Rashid S, Elagan SK. Novel codynamics of the HIV-1/HTLV-I model involving humoral immune response and cellular outbreak: A new approach to probability density functions and fractional operators. AIMS Math. 2023;8(12):28246–79.
[33] Atangana A. Extension of rate of change concept: From local to nonlocal operators withapplications. Res Phys. 2021;19:103515. doi: https://doi.org/10.1016/j.rinp.2020.1.
[34] Atangana A, Gómez-Aguilar JF. Fractional derivatives with no-index law property: Application to chaos and statistics. Chaos Solit Fract. 2018;114:516–35. doi: https://doi.org/10.1016/j.chaos.2018.07.033.
[35] Jarad F, Abdeljawad T, Hammouch Z. On a class of ordinary differential equations in the frame of Atangana-Baleanu fractional derivative. Chaos Solit Fract. 2018;117:16–20. doi: https://doi.org/10.1016/j.chaos.2018.10.006.
[36] Atangana A, Araz SI. New concept in calculus: Piecewise differential and integral operators. Chaos Solit Fract. 2021;145:110638. doi: https://doi.org/10.1016/j.chaos.2020.110638.
[37] Atangana A, Araz SI. Deterministic-stochastic modeling: A new direction in modelingreal world problems with crossover effect, Math Biosci Eng. 2022;19:3526–63. doi: https://doi.org/10.3934/mbe.2022163.
[38] Pérez JES, Aguilar JFG, Atangana A. Novel numerical method for solving V-O fractional differential equations with power, exponential and Mittag-Leffler laws. Chaos Solit Fract. 2018;114:175–85. doi: https://doi.org/10.1016/j.chaos.2018.06.032.
[39] Alkahtani BST, Koca I, Atangana A. A novel approach of variable order derivative: Theory and methods. J Nonlin Sci Appl. 2016;9:4867–76. doi: http://dx.doi.org/10.22436/jnsa.009.06.122.
[40] Atangana A. On the stability and convergence of the time-fractional V-O telegraphequation, J Comput Phys. 2015;293:104–14. doi: https://doi.org/10.1016/j.jcp.2014.12.043.

[41] Atangana A, Baleanu D. New fractional derivatives with nonlocal and non-singular kernel: theory and application to heat transfer model. Therm Sci. 2016;20:763–9. doi: https://doi.org/10.48550/arXiv.1602.03408.
[42] Kumar S, Kumar A, Baleanu D. Two analytical methods for time-fractional nonlinear coupled Boussinesq-Burgeras equations arise in propagation of shallow water waves, Nonlin Dyn. 2016;1:1–17. doi: https://doi.org/10.1007/s11071-016-2716-2.
[43] Zhuang P, Liu F, Anh V, Turner I. Numerical methods for the V-O fractional advectiondiffusion equation with a nonlinear source term. SIAM J Numer Anal. 2009;47:1760–81. doi: https://doi.org/10.1137/080730597.
[44] Nisa KS, Farman M, Abdel-Aty M, Cao J. A review of the singular and non-singular kernels and their applications. Prog Fract Differ Appl. 2023;9:507–44.
[45] Rashid S, Hamidi SZ, Akram S, Aon M, Elagan SK, Alsubei SMT. Theoretical and mathematical codynamics of nonlinear tuberculosis and COVID-19 model pertaining to fractional calculus and probabilistic approach. Sci Rep. 2024;14(1).
[46] Rashid S, Jarad F. Novel investigation of stochastic fractional differential equations measles model via the white noise and global derivative operator depending on Mittag-Leffler kernel. Comp Model Engin Sci. 2024;139(3).
[47] Xu C, Farman M. Dynamical transmission and mathematical analysis for ebola virus in society by using constant proportional operator with power law kernel. Fractal Fractional. 2023;7:706.
[48] Chu YM, Rashid S, Alzahrani T, Alhulayyil H, Alsagri H, Rehman S. Complex adaptive learning cortical neural network systems for solving time-fractional difference equations with bursting and mixed-mode oscillation behaviours. Sci Rep. 2024;13(1).
[49] Du F, Lu JG. New criteria for finite-time stability of fractional order memristor-based neural networks with time delays. Neurocomputing. 2021;421:349–59.
[50] Abdeljawad T, Mert R, Torres DF. Variable order Mittag-Leffler fractional operators on isolated time scales and application to the calculus of variations. In: Fractional derivatives with Mittag-Leffler Kernel. Cham, Switzerland: Springer; 2019. p. 35–47.
[51] You X, Song Q, Zhao Z. Global Mittag-Leffler stability and synchronization of discrete-time fractional-order complex-valued neural networks with time delay. Neural Netw. 2020;122:382–94.
[52] Pratap A, Raja R, Cao J, Huang C, Niezabitowski M, Bagdasar O. Stability of discrete-time fractional-order time-delayed neural networks in complex field. Math Meth Appl Sci. 2021;44:419–40.
[53] Huang LL, Park JH, Wu GC, Mo ZW. Variable-order fractional discrete-time recurrent neural networks. J Comput Appl Math. 2020;370:112633.
[54] Abdeljawad T, Baleanu D. Integration by parts and its applications of a new non-local derivative with Mittag-Leffler non-singular kernel. J Nonlin Sci Appl. 2017;10(3):1098–107.
[55] Abdeljawad T. Fractional operators with generalized Mittag-Leffler kernels and their iterated differintegrals. Chaos. 2019;29(2):023102.
[56] Abdeljawad T, On delta and nabla Caputo fractional differences and dual identities. Discr Dyn Nat Soc. 2013;2013:1–12.
[57] Abdeljawad T. Different type kernel h-fractional differences and their fractional-sums. Chaos Solit Fract. 2018;116:146–56.
[58] Abdeljawad T. Fractional difference operators with discrete generalized Mittag-Leffler kernels. Chaos Solit Fract. 2019;126:315–24.
[59] Al-Qurashi M, Asif QU, Chu YM, Rashid S, Elagan SK. Complexity analysis and discrete fractional difference implementation of the Hindmarsh-Rose neuron system. Res Phys. 2023;51:106627.
[60] Al-Qurashi M, Rashid S, Jarad F, Ali E, Egami RH, Dynamic prediction modelling and equilibrium stability of a fractional discrete bio-physical neuron model. Res Phy. 2023;48:106405.
[61] Baleanu D, Etemad S, Mohammadi H, Rezapour S. A novel modeling of boundary value problems on the glucose graph. Commun Nonlin Sci Numer Sim. 2021;100:105844.
[62] Baleanu D, Jajarmi A, Mohammadi H, Rezapour S. A new study on the mathematical modelling of human liver with Caputo-Fabrizio fractional derivative. Chaos Solit Fract. 2020;134:109705.
[63] Tuan NH, Mohammadi H, Rezapour S. A mathematical model for COVID-19 transmission by using the Caputo fractional derivative. Chaos Solit Fract. 2020;140:110107.
[64] Aydogan SM, Hussain A, Sakar FM. On a nonlinear fractional order model of novel coronavirus (nCoV-2019) under AB-fractional derivative. J Math Extension. 2021;15.
[65] Chu YM, Rashid S, Asif QUA, Abdalbagi M. On configuring new choatic behaviours for a variable fractional-order memristor-based circuit in terms of Mittag-Leffler kernel. Res Phy. 2023;53(1–4):106939.
[66] Peng Y, Liu J, He S, Sun K. Discrete fracmemristor-based chaotic map by Gürunwald-Letnikov difference and its circuit implementation. Chaos Solit Fract. 2023;171:113429.
[67] Ma M, Lu Y, Li Z, Sun Y, Wang C. Multistability and phase synchronization of Rulkov neurons coupled with a locally active discrete memristor. Fractal Fract. 2023;7:82.
[68] Aydogan SM. On a k-dimensional system of hybrid fractional differential equations with multi-point boundary conditions. J Math Extension. 2021;15.
[69] Chu YM, Rashid S, Karim S, Khalid A, Elagan SK. Deterministic-stochastic analysis of fractional differential equations malnutrition model with random perturbations and crossover effects. Sci Rep. 2023;13:14824.
[70] Samei ME, Zanganeh H, Aydogan SM. To investigate a class of the singular fractional integro-differential quantum equations with multi-step methods. J Math Extension. 2021;15.
[71] Chu YM, Rashid S, Karim S, Khalid A, Elagan SK, Deterministic-stochastic analysis of fractional differential equations malnutrition model with random perturbations and crossover effects. Sci Rep. 2023;13:15465.
[72] Khan H, Alam K, Gulzar H, Etemad S, Rezapour S. A case study of fractal-fractional tuberculosis model in China: Existence and stability theories along with numerical simulations. Math Comput Sim. 2022;198:455–73.
[73] Tusi APM, Jones AJ. The control of higher dimensional chaos: comparative results for the chaotic spacecraft attitude control problem. Phys D. 2000;135:41–62.
[74] Kuang J, Tan SH, Leung AYT. Chaotic attitude motion of spacecrafts under small perturbation torques, J Sound Vib. 2000;235:175–200.
[75] Kuang J, Tan S, Arichandran K, Leung AYT. Chaotic dynamics of an asymmetrical gyrostat. Int J Non Linear Mech 2001;36:1213–33.
[76] Kong LY, Zhoul FQ, Zou I. The control of chaotic attitude motion of a perturbed spacecraft. In: Proceedings of the 25th Chinese control conference-2006 Harbin, Heilongjiang, 7-11 Aug, 2006.
[77] Kumar S, Matouk AE, Chaudhary H, Kant S. Control and synchronization of fractional-order chaotic spacecraft systems using feedback and adaptive control techniques. Int J Adapt Control Signal Process. 2020;1–14.

[78] VanDyke MC, Hall CD. Decentralized coordinated attitude control within aformation of spacecraft. J Guid Cont Dyn. 2006;29(5):1101–9.
[79] Liang K, Wang J, Sun Z. Robust decentralized coordinated attitude control ofspacecraft formation, Acta Astronaut. 2011:69(5–6):280–8.
[80] Abdeljawad T, Mert R, Torres DFM, Variable order Mittag-Leffler fractional operators on isolated time scales and application to the calculus of variations. In Fractional Derivatives with Mittag-Leffler Kernel. Cham, Switzerland: Springer; 2019. p. 35–47.
[81] Čermák J, Győri I, Nechvátal L, On explicit stability conditions for a linear fractional difference system. Fract Calc Appl Anal. 2015;18:651–72.
[82] Sadaoui D, Boukabou A, Merabtine N, Benslama M. Predictive synchronization ofchaotic spacecrafts systems. Expert Sys Appl. 2011;38(7):9041–5.
[83] Matignon D, Stability properties for generalized fractional differential systems. In ESAIM: Proceedings. EDP Sciences; 1998. vol. 5. p. 145–58.
[84] Franco-Pérez L, Fernández-Anaya G, Quezada-Téllez LA. On stability of nonlinear nonautonomous discrete fractional Caputo systems. J Math Anal Appl. 2020;487:124021.
[85] Hu QL, Shi YX, Shao XD. Adaptive fault-tolerant attitude control for satellite reorientation under input saturation. Aerosp Sci Tech. 2018;78:171–82.